THE JOURNAL OF PHYSICAL CHEMISTRY B

pubs.acs.org/JPCB Article

Fluorescence Anisotropy Detection of Barrier Crossing and Ultrafast Conformational Dynamics in the S_2 State of β-Carotene

J. K. Gurchiek, Justin B. Rose, Matthew J. Guberman-Pfeffer, Ryan W. Tilluck, Soumen Ghosh, José A. Gascón, and Warren F. Beck*

Cite This: J. Phys. Chem. B 2020, 124, 9029−9046 Read Online

ACCESS | Metrics & More | Article Recommendations | Supporting Information

ABSTRACT: Carotenoids are usually only weakly fluorescent despite being very strong absorbers in the mid-visible region because their first two excited singlet states, S_1 and S_2, have very short lifetimes. To probe the structural mechanisms that promote the nonradiative decay of the S_2 state to the S_1 state, we have carried out a series of fluorescence lineshape and anisotropy measurements with a prototype carotenoid, β-carotene, in four aprotic solvents. The anisotropy values observed in the fluorescence emission bands originating from the S_2 and S_1 states reveal that the large internal rotations of the emission transition dipole moment, as much as 50° relative to that of the absorption transition dipole moment, are initiated during ultrafast evolution on the S_2 state potential energy surface and persist upon nonradiative decay to the S_1 state. Electronic structure calculations of the orientation of the transition dipole moment account for the anisotropy results in terms of torsional and pyramidal distortions near the center of the isoprenoid backbone. The excitation wavelength dependence of the fluorescence anisotropy indicates that these out-of-plane conformational motions are initiated by passage over a low-activation energy barrier from the Franck−Condon S_2 structure. This conclusion is consistent with detection over the 80−200 K range of a broad, red-shifted fluorescence band from a dynamic intermediate evolving on a steep gradient of the S_2 state potential energy surface after crossing the activation barrier. The temperature dependence of the oscillator strength and anisotropy indicate that nonadiabatic passage from S_2 through a conical intersection seam to S_1 is promoted by the out-of-plane motions of the isoprenoid backbone with strong hindrance by solvent friction.

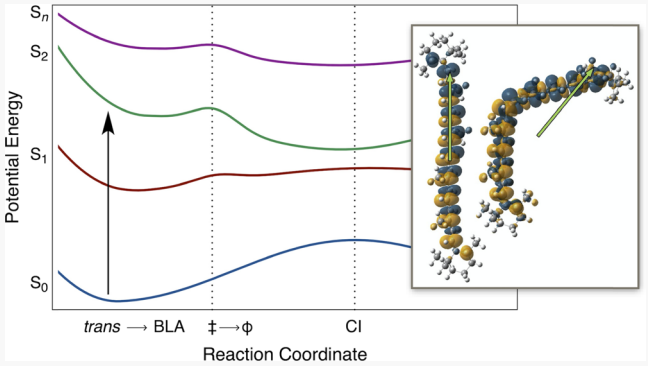

INTRODUCTION

Carotenoids perform essential roles in light harvesting and photoprotection in photosynthetic organisms.[1,2] These functions arise principally from the properties of the two lowest energy excited singlet states, the S_1 and S_2 states.[1,3−5] The S_2 state is optically populated by $\pi \rightarrow \pi^*$ transitions in the strong, mid-visible absorption band, which gives the solutions of the carotenoids a characteristic yellow or orange color. In condensed phases and in the binding sites of proteins, the S_2 state decays usually in <200 fs after absorption of light. Such short lifetimes, on the order of the mid-frequency vibrations of the isoprenoid backbone (Scheme 1), suggest that passage to the S_1 state is mediated by a nonadiabatic mechanism,[6,7] involving strong coupling of the nonradiative electronic transitions to vibrational motions. The fluorescence quantum yield is $\sim 10^{-6}$,[8] much smaller than that of many other $\pi \rightarrow \pi^*$ chromophores. Unusually for the lowest singlet excited states of $\pi \rightarrow \pi^*$ chromophores because it violates Kasha's rule,[9] fluorescence from the S_1 state of carotenoids is weaker than that from S_2 or not observed[10,11] despite the S_1 state's having a much longer lifetime, usually in the ~10 ps range.[3]

The distinct spectroscopic properties of the S_1 and S_2 states in all-*trans* polyenes and carotenoids are usually rationalized in terms of the selection rules for optical transitions of planar structures belonging to the C_{2h} point group.[1] The S_0 and S_2 states are assigned the A_g and B_u characters, respectively, so one-photon electric-dipole transitions between them are fully allowed. However, the S_1 state is assigned the A_g character, so absorption and fluorescence transitions between it and the S_0 state are forbidden by the Laporte rule.[12,13] This scheme is consistent with the finding by Holtom and McClain[14] that the S_1 state of polyenes can be populated from the S_0 state by two-photon optical transitions.[11,15,16]

The nonradiative decay of the S_2 state to the S_1 state of carotenoids has been mainly attributed to the activity in the

Received: July 29, 2020
Revised: September 18, 2020
Published: September 21, 2020

https://dx.doi.org/10.1021/acs.jpcb.0c06961
J. Phys. Chem. B 2020, 124, 9029−9046

Scheme 1. Structure of β-Carotene

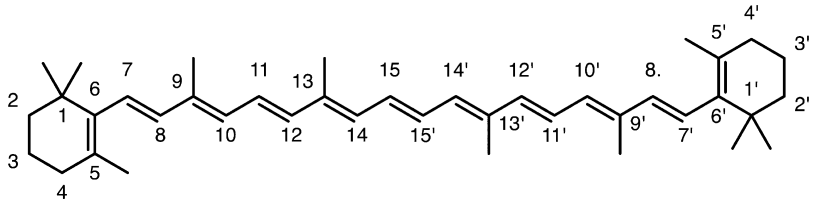

resonance Raman-active C−C and C=C bond-stretching normal coordinates of the isoprenoid backbone. Displacements along these coordinates result in a partial inversion of the carbon−carbon bond-length alternation (BLA) pattern along the isoprenoid backbone upon the optical preparation of the S_2 state and give rise to a vibronic progression in the ground-state absorption spectrum.[1,3,11,17] Relaxation from S_2 to S_1 would involve passage through a conical intersection (CI)[18,19] after a significant displacement from the photoexcited Franck−Condon S_2 structure along the BLA coordinates.[19−21] Because the C_{2h} symmetry would be maintained if only the BLA coordinates are involved, nonradiative decay from S_2 to S_1 would account for quenching of the fluorescence due to the symmetry selection rules. The S_1 state is readily detected in carotenoids, however, by virtue of its strong excited-state absorption (ESA) transitions in the 500−600 nm region, which populate a range of higher energy singlet excited states S_n with B_u character.[22,23]

The S_1 state is nevertheless spectroscopically dark when carotenoids assume asymmetric conformations with symmetries lower than C_{2h}. The ground electronic state, S_0, often favors nonplanar structures in solution; steric clashing of methyl substituents with adjacent isoprenoid backbone results in canting out-of-plane of the β-ionone (cyclohexene) rings of β-carotene and related carotenoids and an overall sigmoidal distortion along the length of the intervening isoprenoid backbone.[24−27] Further, direct one-photon optical preparation of the S_1 state of carotenoids is not observed even when relief from the symmetry selection rules would be expected, such as in structures lacking an inversion center owing to asymmetric substitution,[23] *cis*-stereochemistry,[28] or nonlinear configurations.[29] Overall, these findings raise the argument that the distinct spectroscopic and dynamical properties of the S_1 and S_2 states in carotenoids arise from the underlying details of their electronic structures[30] and from the Franck−Condon overlaps of their potential energy surfaces with the ground state,[29] not as much from simple selection rules determined by symmetry or pseudoparity. The electronic character and the energy ordering[31] of the lowest singlet states of even the shortest polyenes remain controversial because of their considerable theoretical complexity, requiring multireference calculations to achieve chemical accuracy in computational studies.[32−34] The use of multireference calculations to characterize the doubly excited character of the S_1 excited states of carotenoids has been noted in recent work by Mennucci and co-workers.[35,36] Because the carotenoids are large molecules, their potential energy surfaces and CIs have not yet been determined by accurate quantum chemical calculations.

As a further indication of the complexity of the electronic structures of carotenoids, studies of their photophysical properties persistently include mention of several additional dark electronic states at energies adjacent to the S_2 and S_1 states.[1,3] Resonance Raman excitation profiles[37] and time-resolved spectroscopy with broadband, femtosecond pulses[38−41] have implicated one of these dark states, S_x, in mediating nonradiative transfer of population from the S_2 state to the S_1 state. There are two current proposals for the nature of the S_x state.[3,4] The first assigns the S_x state to a discrete singlet excited state with an energy lying below that of the bright S_2 state.[38] In the scheme introduced by Tavan and Schulten,[42] this state would have B_u character in the C_{2h} point group.

An alternative recent proposal is that the S_x state is actually a dynamic intermediate moving on the S_2 state surface along the out-of-plane vibrational coordinates of the isoprenoid backbone.[4] This hypothesis accounts for several key aspects of the femtosecond time evolution of the ESA signals from β-carotene observed by Cerullo et al.[38] and of the heterodyne transient grating signals from β-carotene and the ketocarotenoid peridinin observed in our laboratory.[43,44] As sketched in Figure 1 in terms of schematic potential energy surfaces, an initial excursion along the BLA coordinates after absorption of a photon would drive the molecule in less than a vibrational period to the vicinity of a low activation energy barrier, which divides regions of the S_2 potential energy surface for planar and out-of-plane distorted conformations. Crossing the barrier leads to a steep potential energy gradient with respect to the torsional and/or pyramidal coordinates of the isoprenoid backbone.[4,43−45] The presence of the barrier was initially suggested[4] in analogy to that determined by electronic structure calculations of the potential energy surfaces for the $\pi \rightarrow \pi^*$ excited states of models for retinal protonated Schiff bases (PSBs) and of medium-conjugation length cyanines.[46]

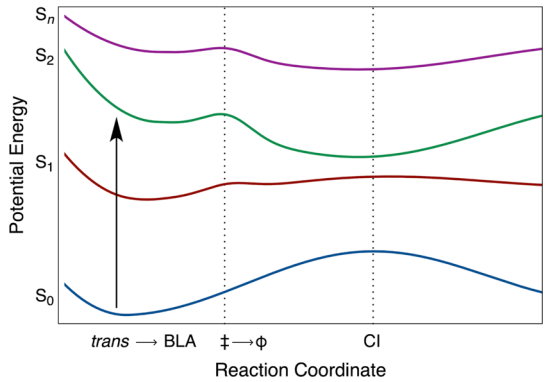

Figure 1. Schematic potential energy curves[4,43,48] proposed for the singlet excited states of all-*trans*-β-carotene, as plotted with respect to a reaction coordinate for the structural response following the optical preparation of the S_2 state. An activation-energy barrier (‡) divides planar (BLA coordinates) and out-of-plane distorted (torsional and/or pyramidal coordinates, φ) regions of the potential energy surfaces. The S_2 and S_1 surfaces strongly interact at a CI seam near the S_2 minimum with respect to the φ coordinates.

https://dx.doi.org/10.1021/acs.jpcb.0c06961
J. Phys. Chem. B 2020, 124, 9029−9046

Qualitatively, the barrier height would be expected to increase with longer polyenes because the π^* character per bond would accordingly decrease; for ethene, the potential energy surface is barrierless.[47]

Following the barrier, the proposed S_2 and S_1 potential curves are depicted as converging along the out-of-plane coordinates at a seam of CIs,[19,31] where the two states are expected to be strongly mixed. Instead of the harmonic single-coordinate picture discussed in previous work, the photophysics of carotenoids is discussed in this hypothesis in terms of anharmonic multicoordinate dynamics. The shape of the S_1 potential energy curve suggested in Figure 1 follows the main features of that proposed by de Weerd et al.[48] in a discussion on their femtosecond pump−continuum probe results, but we have added a low barrier at the onset of torsions corresponding to that proposed for the S_2 state. Because the S_1 state has a doubly excited character, corresponding to two spin-coupled triplet excitations,[31] the barrier height would be expected to be lower than that of the S_2 state, which is a singly excited state. The results of de Weerd et al. suggest that the S_1 state should exhibit a global minimum near the planar, all-*trans* structure. Accordingly, crossing from the S_2 state to the S_1 state near the CI seam would usually be followed by conformational relaxation back to the planar structure. This aspect is consistent with the recent suggestion by Wei et al.[30] that the S_1 state of carotenoids should be conformationally stiffer (e.g., favoring planar structures) than the S_2 state. In a minor fraction of photoexcitations, of course, this scheme anticipates that relaxation from the CI would occur to the *cis* configuration on the S_0 surface after internal conversion from the S_1 state. We need to reiterate, however, that these aspects of the S_2 and S_1 potentials are merely hypotheses that are consistent with some, but not necessarily all, of the currently available experimental information.

S_x is detected in heterodyne transient grating spectra as a dynamic intermediate, following the decay of the stimulated emission (SE) from the Franck−Condon S_2 state and prior to the rise of the strong ESA from the S_1 state.[43] For peridinin, we found that the lifetime of S_x in a range of solvents exhibits a power law dependence with respect to the viscosity or the polar solvation time of the solvent. This behavior indicates that radiationless decay from the S_x intermediate on the S_2 surface to the S_1 state is promoted by large-amplitude out-of-plane distortions of the isoprenoid backbone, with the polar solvation dependence implicating the formation of an intramolecular charge-transfer (ICT) character.[45] The changes in electronic structure that accompany twisting and pyramidal distortions of a isoprenoid backbone have been extensively discussed by Bonačić-Koutecký et al.[49−51] In peridinin, the electron-withdrawing tendency of the carbonyl substituent on the γ-lactone ring in conjugation with the isoprenoid backbone would be expected to enhance the ICT character significantly, which would increase the solvent friction for the motions that promote decay to the S_1 state. This proposal accounts for the observation that the lifetime of the S_x state of peridinin is substantially longer than that of β-carotene, which lacks a carbonyl substituent.[45]

An important implication of the assignment of S_x to a dynamic intermediate in the S_2 state is that the spontaneous fluorescence and SE signals should evolve rapidly to longer wavelengths, well into the near-IR, as molecules descend along the out-of-plane potential energy gradient. The femtosecond pump−probe experiments and global target modeling by de Weerd et al.[48] suggested this possibility for β-carotene early on. The SE from the S_2 state is red shifted from the ground-state bleaching signal at short time delays following photoexcitation, but at longer time delays, it is partially obscured by a much stronger ESA band at longer wavelengths. This time evolution to the red was interpreted in terms of progress along a torsional potential energy gradient, which would narrow the energy gap between the S_2 and S_1 surfaces as they converge at a CI. In a recent work, Liebel et al.[52] used femtosecond transient absorption spectroscopy to observe in β-carotene that passage through the CI between the S_2 and S_1 states occurs with retention of vibrational coherence in modes that lack resonance Raman activity. In Figure 1, the out-of-plane coordinates lack resonance Raman activity because the gradient is accessed only after a significant displacement with respect to the BLA coordinates.

In the present study, we report a test of this picture for the light-induced dynamics in carotenoids using the continuous-wave line shape, quantum yield, and anisotropy of the fluorescence emission from β-carotene in several aprotic solvents. Emission from molecules moving on a gradient on the S_2 potential energy surface with respect to out-of-plane coordinates after passage over a low activation energy barrier gives rise to a broad fluorescence spectrum with a low anisotropy, with the anisotropy decreasing as the excitation source is scanned to the blue over the vibronic structure of the absorption spectrum from the 0−0 region. A weaker fluorescence spectrum with partially resolved vibronic structure arising from the S_1 state is detected in the near-IR, and it also exhibits a strong intensity dependence on the excitation wavelength. The minimum fluorescence anisotropy detected at long emission wavelengths is consistent with a large internal rotation of the emission transition dipole moment (TDM), as much as 50° in nonpolar solvents. Because the TDM is aligned within a few degrees of the molecular frame of the isoprenoid backbone in all-*trans* polyenes,[16,53,54] these results indicate directly that β-carotene undergoes large-amplitude out-of-plane conformational motions as nonradiative decay from the S_2 state to the S_1 state occurs. This picture is further supported by studies of the fluorescence emission at low temperatures, which show that it is possible to observe stronger emission from a dynamic intermediate evolving on the S_2 state that may correspond to S_x or to its precursor from the photoexcited, Franck−Condon structure. Companion electronic structure calculations are then used to determine how the permanent dipole moment and the rotation of the emission TDM are induced by torsional and pyramidal distortions of the isoprenoid backbone. These calculations suggest that the fluorescence anisotropy results are consistent with a zwitterionic structure with a pyramidal conformation in the center of the isoprenoid backbone.

METHODS

Sample Preparation. β-carotene from Sigma/Aldrich (C9750-5G) was purified by Amy LaFountain in the Frank laboratory at the University of Connecticut by high-performance liquid chromatography (HPLC) on a Waters 600E/600S multisolvent delivery system equipped with a 2996 photodiode array detector, as described previously.[55] Additional details are provided in the Supporting Information. After removal of the solvent under a stream of nitrogen gas, the purified β-carotene samples were stored in darkness in a −70 °C freezer. For the present experiments, the β-carotene samples were removed

https://dx.doi.org/10.1021/acs.jpcb.0c06961
J. Phys. Chem. B 2020, 124, 9029−9046

from cold storage, divided into aliquots, and then dissolved in a particular solvent to obtain an absorbance of 0.2 at the peak of the absorption spectrum (460 nm in hexane) for a 1 cm optical path length. The samples were then centrifuged at 17000*g* in a desktop microcentrifuge for 10 min to remove light-scattering particles. The samples were held in 1 cm fused-silica cuvettes either in a Quantum Northwest Peltier-effect temperature controller or in a Janis liquid nitrogen cryostat (for $T < 200$ K).

Absorption Spectroscopy. Room temperature (23 °C) absorption spectra were recorded with a Shimadzu UV-2600 spectrophotometer with a spectral bandpass of 2 nm. With fluorescence samples mounted in the Peltier-effect temperature controller or the liquid nitrogen cryostat, absorption spectra were recorded in situ at the indicated temperature with a single-beam spectrometer, which was assembled from an Ocean Optics DH-2000 light source, Ocean Optics QP400-1-UV−VIS fiber optic cables, and an Ocean Optics USB4000 spectrograph/CCD detector (0.1 nm bandpass).

Fluorescence Spectroscopy. Fluorescence spectroscopy with continuous excitation was performed with a home-built spectrometer incorporating a broadband LED and a compact double monochromator (2 nm bandpass) for the excitation light source. A grating spectrograph with a 0.15 m focal length (4 nm bandpass) and a back-illuminated CCD detector was used as the detection system. This instrument is an improved setup based on the one we described previously.[56] The orientations of the linear planes of polarization of the excitation and emission beams were selected using calcite Glan−Thompson and Glan−Taylor polarizers, respectively, with the latter mounted in a motorized rotation stage. The emission spectra were corrected for the wavelength dependences of the emission optics, spectrograph, and CCD detector. The details of the instrumentation and of the protocols used to measure the fluorescence emission and anisotropy are reported in the Supporting Information. The spectra shown in this paper were acquired with very low intensity excitation beams (for example, 5.86 μW at 460 nm), and the samples were repeatedly allowed to recover in darkness during the acquisition of dark background spectra prior to the recording of additional spectra. Each reported spectrum was obtained as the average, after the scan-to-scan rejection of cosmic ray spikes, of 16 four-minute exposures of the CCD camera for a given polarization state. Figure S2 presents the fluorescence emission and anisotropy spectra from rhodamine 6G in glycerol, which was employed as a reference sample for the quantum yield and anisotropy measurements.

The absorption spectrum of the β-carotene samples was measured before and after the fluorescence data acquisition cycle to determine whether permanent photobleaching occurred or whether photoproducts were accumulated. The photobleaching of β-carotene due to the formation of radical cation species via photoinduced charge transfer reactions[57] has been detected in chloroform solutions via near-IR absorption transients.[58,59] No changes in absorption were detected in any of the samples monitored during these experiments.

Electronic Structure Calculations. Electronic structure calculations were performed with the B3LYP hybrid functional,[60,61] a 6-31G(d) basis set, and an ultrafine grid for integration, as implemented in Gaussian 16 revision A.01.[62] As discussed below, relaxed potential energy scans were conducted around each double bond of β-carotene and of those in a truncated analogue in which the β-ionone rings were replaced by hydrogens. These scans were conducted around each bond by varying the dihedral angle from 180 to 90°. The all-*trans* and twisted conformers were subjected to time-dependent density functional theory (TD-DFT) calculations under the Tamm−Dancoff approximation using the CAM-B3LYP/6-31G(d) model chemistry.[63] For full-length, all-*trans* β-carotene, this level of theory delivers an $S_0 \rightarrow S_2$ vertical excitation energy within ~0.08 eV (~12 nm) of the experimental absorption maximum at 460 nm. This combination of two different levels of DFT and/or basis sets, one for ground state optimization and the other for excited state energies, has been used before and particularly in the context of carotenoids.[35,36] The transition density for the $S_0 \rightarrow S_2$ excitation was generated with MultiWFN[64] and visualized in Gaussview.

RESULTS

Fluorescence Spectra. Figure 2 compares the room temperature (23 °C) absorption spectrum with the fluorescence spectra observed at four excitation wavelengths from β-carotene in hexane solvent. As discussed previously by Gillbro and Cogdell,[8] the fluorescence and absorption spectra overlap over the ~480−520 nm region, which is consistent with an assignment of the emission to the S_2 state. Owing to the low quantum yield, $\sim 10^{-6}$, the broad fluorescence lineshape is decorated with sharper line shapes arising from light scattering at the excitation wavelength, from resonance Raman scattering at the C−C and C=C mode frequencies, and from nonresonance Raman scattering from the hexane solvent. The Raman signals move at fixed Stokes shifts (in wavenumbers) as the excitation wavelength is scanned across the absorption spectrum, revealing as they move that the obscured part of the fluorescence line shape lacks any resolved vibronic structure. In contrast, the absorption spectrum exhibits a partially resolved vibronic progression in the BLA coordinates. This observation indicates that the optically

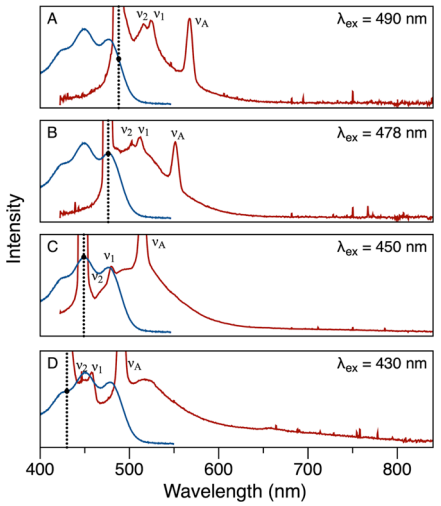

Figure 2. Absorption (blue) and fluorescence emission (red) spectra at four excitation wavelengths from β-carotene in hexane solvent at 23 °C. For the fluorescence spectra, the emission polarizer was oriented at the magic angle (54.6°) with respect to the excitation polarizer. The excitation wavelength is marked in each panel with a vertical dashed line. The positions of resonance Raman peaks from β-carotene (ν_1 = 1517 cm^{-1} and ν_2 = 1157 cm^{-1})[66] and of a nonresonance Raman peak from the hexane solvent (ν_A = 2966 cm^{-1})[67] are marked.

https://dx.doi.org/10.1021/acs.jpcb.0c06961
J. Phys. Chem. B 2020, 124, 9029−9046

prepared S_2 state abruptly undergoes a change in the electronic structure that increases the solvation reorganization energy (or system−bath coupling). Simulations of the absorption and fluorescence spectra using the multimode Brownian oscillator (MBO) model[65] are presented in the Supporting Information. The absorption transition would be expected to impact the chromophore−solvent interactions by increasing the chromophore's permanent dipole moment and/or the molecular size relative to that of the surrounding solvent cavity.

As the excitation wavelength is scanned from the 0−0 region (Figure 2a) over the vibronic structure of the absorption spectrum (Figure 2b−d), the fluorescence spectrum exhibits a significant broadening in the emission bandwidth. In particular with excitation at 450 nm (Figure 2c) or 430 nm (Figure 2d), the emission is strengthened especially in the near-IR, >600 nm region. The origin of the broadening is made clearer by comparing the 490 and 430 nm spectra replotted as the emission oscillator strength in comparison with the fluorescence anisotropy (Figure 3).

The oscillator (or dipole) strengths $\varepsilon(\nu)/\nu$ and $\lambda^2 F(\nu)/\nu^3$ express the squares of the absorption and fluorescence transition probabilities[68,69] with respect to the wavenumber, ν, as determined by the absorption and the fluorescence intensity, $\varepsilon(\nu)$ and $F(\nu)$, respectively, and with λ standing for the wavelength.[70−73] In Figure 3, the fluorescence oscillator strength spectra obtained with excitation at 490 and 430 nm are plotted with consistent scaling factors after normalizing them for the excitation light intensity. The tuning of the excitation wavelength to 430 from 490 nm substantially increases the oscillator strength of the fluorescence emission across the entire detection range but especially below ∼18,000 cm^{-1}.

The oscillator strength spectra make it clear that a second fluorescence band is superimposed on the tail of the main emission band from S_2. This second band is assigned to emission from the S_1 state following nonradiative decay from S_2. The contribution from the S_1 fluorescence band is not nearly as obvious in the intensity spectra plotted in Figure 2 due to the effective attenuation by the fixed wavelength bandpass of the emission spectrograph. Although the signal/noise ratio is relatively poor in this region of the spectrum owing to the decreasing sensitivity at long wavelengths of the silicon CCD detector used in these experiments, one can discern the weak emission band from S_1 in the spectrum obtained with 490 nm excitation (Figure 2a) from its apparent peak maximum in the ∼12,500−13,000 cm^{-1} range. A weak S_1 spectrum from β-carotene in carbon disulfide in this wavenumber region was detected previously with a germanium detector and with laser excitation by Andersson et al.[74]

The S_1 band observed with excitation at 430 nm (Figure 2b), however, is substantially stronger than that observed with 490 nm excitation. Its line shape is broader, extending at least from 18,000 cm^{-1} to the low-frequency limit of the detected spectra, and its peak maximum is markedly blue shifted. Further, the intensity is modulated over the 13,500−14,000 cm^{-1} range, which may arise from partially resolved vibronic structure. The S_1 fluorescence spectrum reported by Andersson et al.[74] was assigned a weak vibronic progression in the BLA mode frequencies.

Fluorescence Anisotropy Spectra. The fluorescence anisotropy, r, is calculated from the linear polarization emission components detected parallel and perpendicular to the plane of polarization of the excitation light, $F_{\parallel}$ and $F_{\perp}$, as

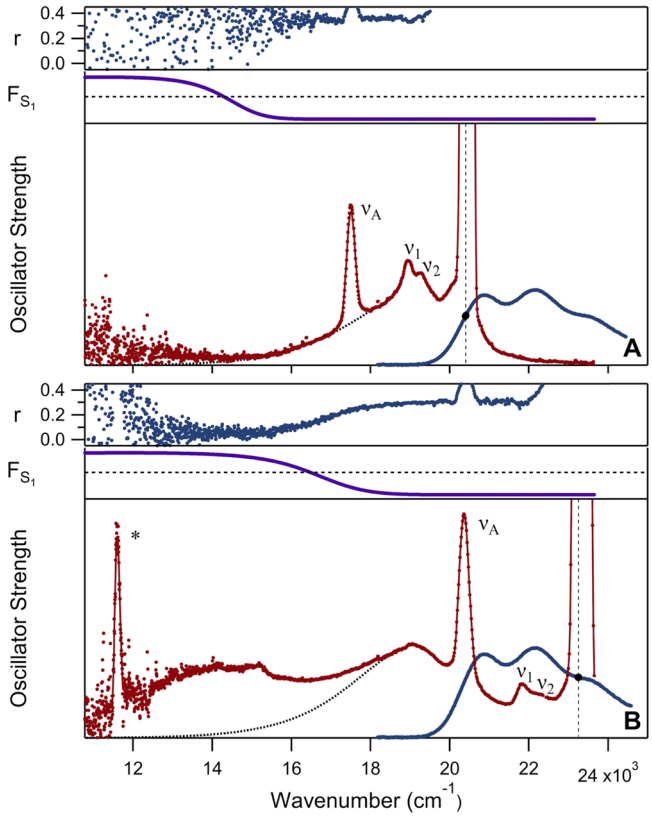

Figure 3. Fluorescence oscillator strength and anisotropy (r) spectra for β-carotene in hexane at 293 K: (a) with excitation at 490 nm (20,400 cm^{-1}) and (b) with excitation at 430 nm (23,250 cm^{-1}). The magic-angle fluorescence oscillator strength (red) is plotted after correction for the intensity of the excitation light at the two wavelengths with the same intensity scaling in panels (a) and (b). The excitation wavenumber is marked in each panel with a vertical dashed line. The absorption oscillator strength (blue) is arbitrarily scaled to mirror that of the S_2 fluorescence emission line shape. A baseline for the S_1 emission (dotted curve) is suggested by a lognormal lineshape for the red tail of the S_2 emission. F_{S1} (purple) estimates the fraction of the fluorescence oscillator strength from the S_1 state; F_{S1} = 0.5 is marked by the dashed line. The positions of resonance Raman peaks from β-carotene (ν_1 = 1517 cm^{-1} and ν_2 = 1157 cm^{-1})[66] and of a nonresonance Raman peak from the hexane solvent (ν_A = 2966 cm^{-1})[67] are marked. Also marked (*) is the second-order excitation light scattering peak.

$$r = \frac{F_{\parallel} - F_{\perp}}{F_{\parallel} + 2F_{\perp}} \quad (1)$$

The anisotropy reports the angle θ between the emission and absorption TDMs, the latter as photoselected from the randomly oriented ground-state ensemble present in solution,[69]

$$r = r_0 P_2(\theta) = r_0(3\cos^2\theta - 1)/2 \quad (2)$$

In this equation, r_0 is the maximum anisotropy, 0.4, which corresponds to parallel TDM directions for the absorption and emission TDMs, and P_2 is the second Legendre polynomial. As the emission TDM is rotated away from alignment with the absorption TDM, the anisotropy decreases. A complete loss of memory of the photoselected absorption TDM direction due to rotational diffusion would result in a full depolarization of the fluorescence emission and an anisotropy of 0.0, but the rotational correlation time measured for β-carotene in hexane

https://dx.doi.org/10.1021/acs.jpcb.0c06961
J. Phys. Chem. B 2020, 124, 9029−9046

determined using optical Kerr effect measurements is 115 ps at 20 °C.[75] Depolarization of the fluorescence from S_2 from rotational diffusion is entirely negligible owing to the <150 fs lifetime of the S_2 state. Further, for the S_1 emission, at most a 5% decrease in the fluorescence anisotropy would accompany rotational diffusion averaged over the 10 ps lifetime[22,43,76,77] of the S_1 state. Thus, fluorescence anisotropies much lower than 0.4 arise in β-carotene from an internal rotation of the emission TDM relative to the photoselected direction of the absorption TDM.

The fluorescence anisotropy spectra plotted in Figure 3 decrease monotonically as the emission frequency extends into the near-IR region except in the neighborhood of Raman scattering features, which are highly polarized. This trend indicates that the fluorescence from the S_1 state exhibits a lower anisotropy than the S_2 state. The contribution of the fluorescence from the S_1 state to the measured anisotropy at a given wavenumber can be estimated from the fraction of the total oscillator strength at a given wavenumber from the S_1 state, F_{S1}, which is plotted above the main oscillator strength panels in Figure 3. Lognormal lineshapes[78] were applied here to estimate the oscillator strength from the S_2 state where it overlaps with that from the S_1 state; a similar approach was used by Andersson et al.[74]

With excitation at 490 nm (Figure 3a), the minimum anisotropy observed in the S_2 emission region at 16,500 cm^{-1} is ~0.35, which indicates only a 17° rotation of the emission TDM from the direction of the vertical absorption TDM using eq 2. A similar anisotropy value extends across the weak S_1 emission region, though the signal/noise ratio is very poor. With excitation at 430 nm (Figure 3b), however, the anisotropy is as low as 0.28 in the S_2 region, implying a rotation of the emission TDM by 26°. An even lower anisotropy is then observed in the S_1 region, 0.05, corresponding to a rotation of the TDM of almost 50°. These results make it clear that tuning the excitation wavelength to shorter wavelengths over about a 3000 cm^{-1} range from the 0−0 transition results in an increased rotation of the emission TDM in both the S_2 and the S_1 bands. Additional fluorescence anisotropy spectra from β-carotene in hexane showing this trend are presented in the wavelength spectra provided in the Supporting Information.

Solvent Dependence of the Fluorescence Emission and Anisotropy from β-Carotene. We carried out additional studies of the fluorescence properties of β-carotene in three additional aprotic solvents affording comparable solubility to that in hexane:chloroform (Figure 4), 2-methyltetrahydrofuran (2-MTHF, Figure 5), and carbon disulfide (Figure 6). These figures present the fluorescence oscillator strength and anisotropy spectra in these solvents in the same manner used above in Figure 3 for β-carotene in hexane. The Supporting Information presents the wavelength plots of the fluorescence emission and anisotropy spectra for these solvents as the excitation wavelength is tuned over the vibronic structure of the ground-state absorption spectrum. The fluorescence quantum yields and minimum anisotropies in the S_2 and S_1 fluorescence bands in each of the four solvents are compared in Table 1. The reported anisotropies are the minimum values observed in the spectral regions assigned to the S_2 and S_1 bands, estimated as discussed above as guided by the apparent fraction of the emission oscillator strength from S_1, F_{S1}. For S_2 we chose to measure the anisotropy at Stokes

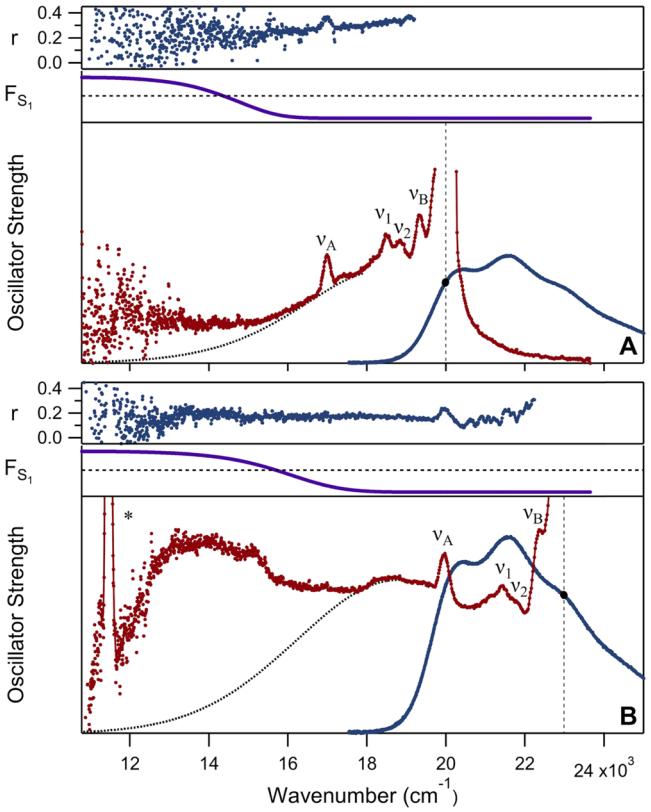

Figure 4. Fluorescence oscillator strength and anisotropy (r) spectra for β-carotene in chloroform at 293 K: (a) with excitation at 500 nm (20,000 cm^{-1}) and (b) with excitation at 435 nm (23,000 cm^{-1}). Other details are as indicated in the caption to Figure 3, including plotting the fluorescence oscillator strength spectra with the same intensity scaling in panels (a) and (b). The positions of resonance Raman peaks from β-carotene (ν_1 = 1517 cm^{-1} and ν_2 = 1157 cm^{-1})[66] and nonresonance Raman peaks from the chloroform solvent (ν_A = 2966 cm^{-1} and ν_B = 732 cm^{-1})[79] are marked.

shifts above ~3500 cm^{-1} so as to avoid regions where Raman scattering would be expected.

The trends in fluorescence lineshape, oscillator strength, and anisotropy described above for β-carotene in hexane that accompany the tuning of the excitation wavelength over the ~3000 cm^{-1} region above the 0−0 absorption transition are also observed in the three additional solvents. In chloroform (Figure 4b) and 2-MTHF (Figure 5b), the S_1 emission exhibits some weakly resolved vibronic structure; in contrast, the S_1 emission observed in carbon disulfide (Figure 6b) displays less vibronic structure but is perhaps 10 times more intense than observed in the other solvents. In all three solvents, the S_2 fluorescence anisotropy is ~0.2, somewhat lower than that observed in hexane, whereas the fluorescence anisotropy from the S_1 state is significantly lower in the nonpolar solvents, ~0.06, compared to that in the polar solvents, ~0.15.

Several aspects of the results reported above have been observed previously by other workers, but the fluorescence line shape and anisotropy properties were not simultaneously connected in any prior work, to our knowledge. Gillbro and Cogdell[8] reported a decrease in the fluorescence emission anisotropy from β-carotene in carbon disulfide at a single emission wavelength, 570 nm, as the excitation wavelength was scanned to the blue over the 500−400 nm range; fluorescence emission spectra over this excitation tuning range were not

https://dx.doi.org/10.1021/acs.jpcb.0c06961
J. Phys. Chem. B 2020, 124, 9029−9046

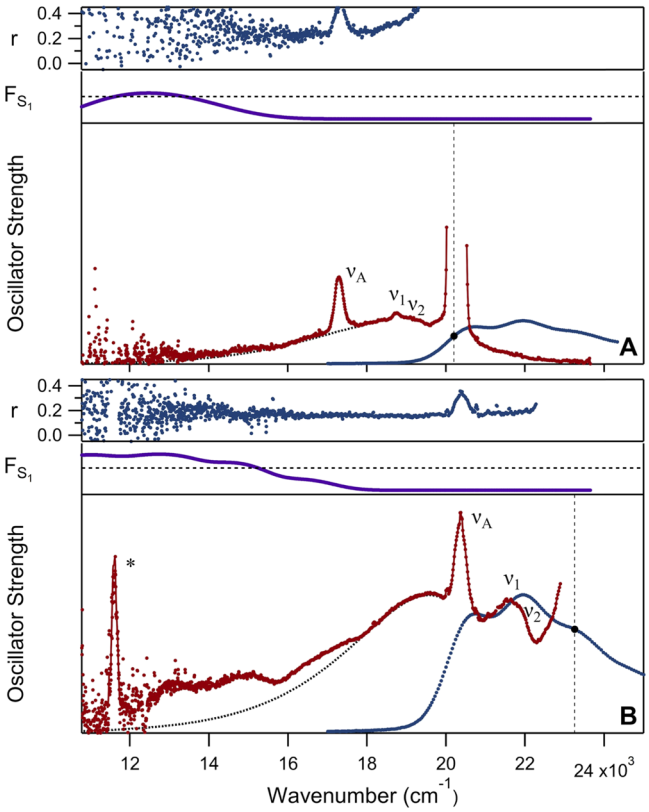

Figure 5. Fluorescence oscillator strength and anisotropy (r) spectra for β-carotene in 2-MTHF at 293 K: (a) with excitation at 495 nm (20,200 cm^{-1}) and (b) with excitation at 430 nm (23,250 cm^{-1}). Other details are as indicated in the caption to Figure 3, including plotting the fluorescence oscillator strength spectra with the same intensity scaling in panels (a) and (b). The positions of resonance Raman peaks from β-carotene (ν_1 = 1517 cm^{-1} and ν_2 = 1157 cm^{-1})[66] and of a nonresonance Raman peak from the 2-MTHF solvent (ν_A = 2915 cm^{-1})[80] are marked.

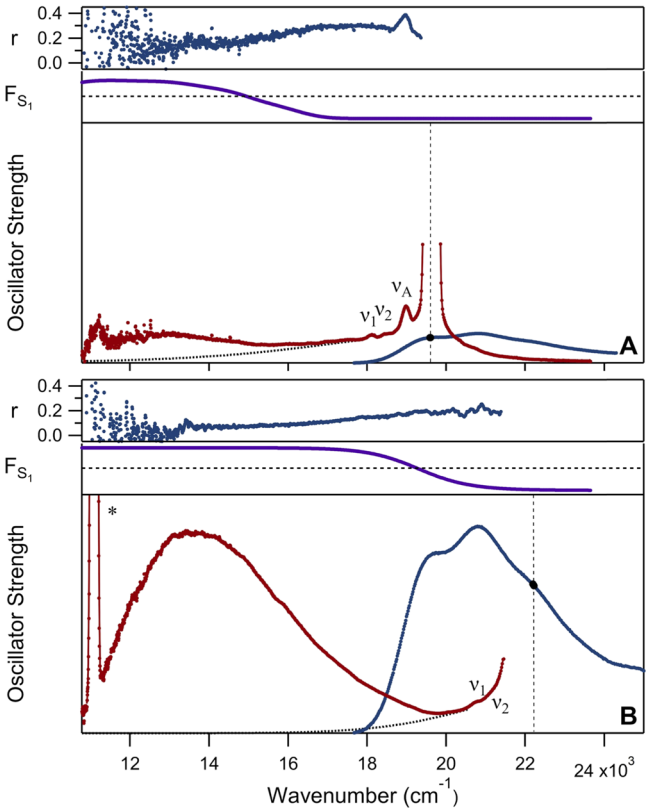

Figure 6. Fluorescence oscillator strength and anisotropy (r) spectra for β-carotene in carbon disulfide at 293 K: (a) with excitation at 510 nm (19,600 cm^{-1}) and (b) with excitation at 450 nm (22,200 cm^{-1}). Other details are as indicated in the caption to Figure 3, including plotting the fluorescence oscillator strength spectra with the same intensity scaling in panels (a) and (b). The positions of resonance Raman peaks from β-carotene (ν_1 = 1517 cm^{-1} and ν_2 = 1157 cm^{-1})[66] and of a nonresonance Raman peak from the CS_2 solvent (ν_A = 658 cm^{-1})[81] are marked.

shown. The results described above for the S_2 emission are in line with their findings. To explain the anisotropy decrease, Gillbro and Cogdell proposed that the absorption spectrum contains two overlapping bands with distinct emission TDM directions. A similar argument was made by Oustramov et al.[40] to account for their observation that the fluorescence line shape of β-carotene deviates from mirror symmetry and from that expected from the Stepanov relation, which assumes that no structural rearrangements occur from the Franck−Condon structure and that the emission arises from the lowest vibrational level of the emitting state.[82] In fact, it was concluded in this work that the majority of the fluorescence emission with excitation near the 0−0 transition arises from optical preparation of the low-lying B state of Tavan and Schulten mentioned in the Introduction. Tuning of the excitation into the blue wavelengths associated in the present work with the near-IR fluorescence was not reported nor was there any discussion of fluorescence anisotropy results.

We should point out at this point that the possible presence of overlapping transitions in the mid-visible absorption band of β-carotene does not really provide a satisfactory physical explanation for the correlated changes observed here in the fluorescence line shape and anisotropy. As shown below in the electronic structure calculations and consistent with previous work,[16,74] the TDMs of all-*trans* carotenoids are well aligned longitudinally with the direction of the isoprenoid backbone. A contribution from $\pi \rightarrow \pi^*$ transitions with TDM components in the transverse direction would be expected to be blue shifted from the main band and much weaker in oscillator strength. Further, linear dichroism spectra indicate that photoselection of ground-state molecules with cis configurations does not occur over the 430−500 nm excitation range.[83] The *cis* band in β-carotene is located at shorter wavelengths, ∼300−350 nm.[84]

Temperature Dependence of the Fluorescence from β-Carotene. An alternative explanation for the fluorescence anisotropy results is that the isoprenoid backbone of β-carotene undergoes out-of-plane distortions that rotate the emission TDM while still evolving on the S_2 potential energy surface during the <150 fs emission timescale.[4,43] The excitation wavelength dependence of the fluorescence anisotropy would then indicate that passage over a low activation barrier from the Franck−Condon region of the S_2 state's potential energy surface, as depicted in Figure 1, is required to access to the potential energy gradient with respect to out-of-plane motions. Further, the lower anisotropy observed in the S_1 fluorescence band would be explained by an additional internal rotation of the emission TDM that follows passage through the CI from the S_2 state.

A test of the possible assignments for the fluorescence anisotropy of β-carotene can be made by performing a series of

https://dx.doi.org/10.1021/acs.jpcb.0c06961
J. Phys. Chem. B 2020, 124, 9029−9046

Table 1. Fluorescence Quantum Yield and Anisotropy Parameters for β-Carotene

solvent	λ_{exc} (nm)	$\Phi_{F,S2}$ [a]	$\Phi_{F,S1}$ [a]	r_{S2} [b]	θ_{S2} [c]	r_{S1} [b]	θ_{S1} [c]
n-hexane	430	1.7×10^{-6}	6.8×10^{-7}	0.28 ± 0.01	26.6 ± 2.4°	0.05 ± 0.04	49.8 ± 5.8°
	490	1.1×10^{-6}	3.2×10^{-8}	0.35 ± 0.04	16.8 ± 15.4°		
carbon disulfide	450	5.7×10^{-6}	1.7×10^{-5}	0.20 ± 0.02	35.3 ± 4.1°	0.07 ± 0.01	47.9 ± 1.9°
	510	1.9×10^{-6}	7.0×10^{-7}	0.29 ± 0.01	25.4 ± 2.5°	0.14 ± 0.05	41.2 ± 9.7°
chloroform	435	3.8×10^{-6}	8.6×10^{-7}	0.16 ± 0.01	39.2 ± 1.9°	0.14 ± 0.11	41.2 ± 21.7°
	500	1.1×10^{-6}	1.2×10^{-7}	0.25 ± 0.02	30.0 ± 4.4°	0.24 ± 0.16	31.1 ± 46.9°
2-MTHF	430	2.0×10^{-6}	4.7×10^{-7}	0.16 ± 0.01	39.2 ± 1.9°	0.17 ± 0.10	38.3 ± 21.1°
	495	7.3×10^{-7}	2.6×10^{-8}	0.24 ± 0.03	31.1 ± 6.5°		

[a]Absolute fluorescence quantum yield. [b]Minimum fluorescence anisotropy at long wavelengths for the indicated emission band (Figures 4, 6, 8, and 10). [c]Rotation angle of the fluorescence emission TDM from the photoselected TDM for the absorption transition, from eq 2.

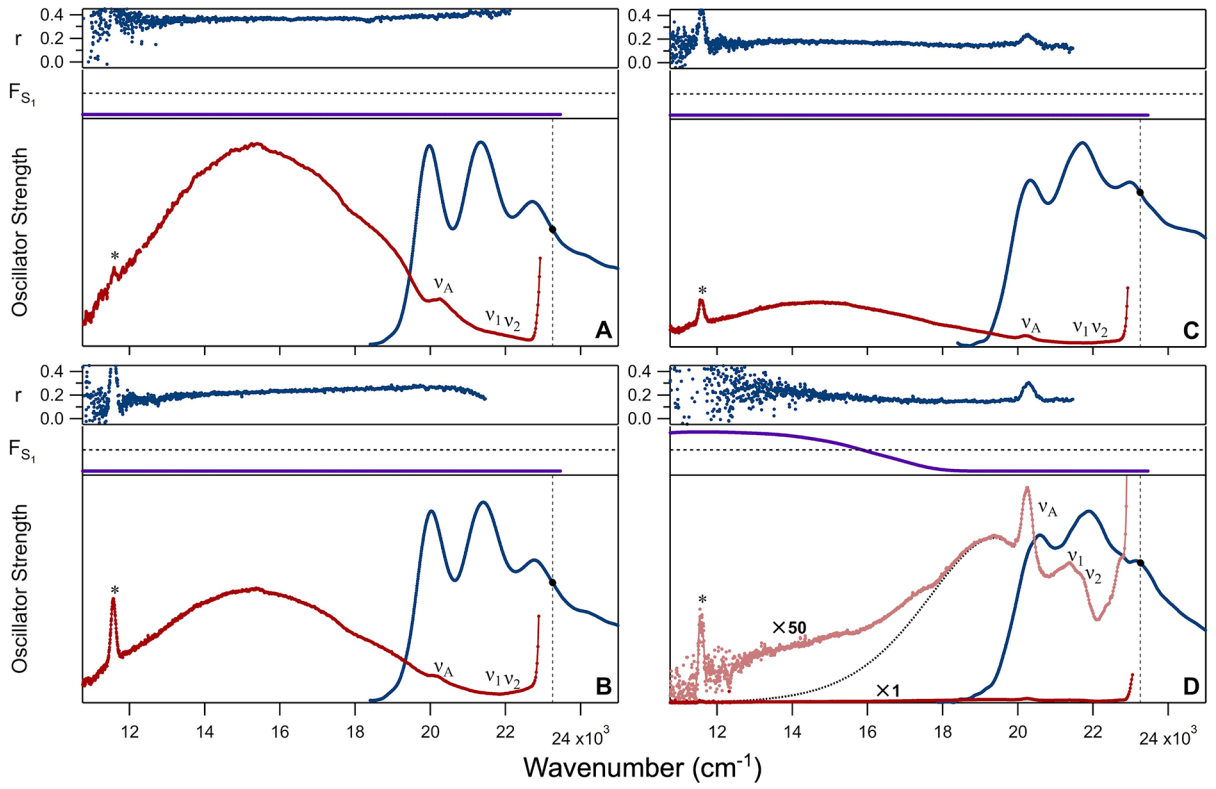

Figure 7. Absorption (blue) and fluorescence (red) oscillator strength and anisotropy (r) spectra for β-carotene in 2-MTHF with excitation at 430 nm (23,250 cm^{-1}) at: (a) 80 K; (b) 120 K; (c) 200 K; and (d) 258 K. Other details are as indicated in the caption to Figure 3, including plotting the fluorescence oscillator strength spectra with the same intensity scaling in all four panels. In (d), the fluorescence oscillator strength is also replotted at ×50 scaling. The positions of resonance Raman peaks from β-carotene (ν_1 = 1517 cm^{-1} and ν_2 = 1157 cm^{-1})[66] and of a nonresonance Raman peak from the 2-MTHF solvent (ν_A = 2915 cm^{-1})[80] are marked.

fluorescence observations as a function of temperature. At low temperatures, a high fluorescence anisotropy would be expected if the friction from the surrounding frozen solvent inhibits large amplitude out-of-plane motions from the Franck−Condon S_2 state structure. On the other hand, if tuning of the excitation wavelength to shorter wavelengths changes the fluorescence line shape or anisotropy because of coming into resonance with a low-lying B state, the alternative assignment suggested above, the same anisotropy value would be anticipated at low and higher temperatures. Lowering the temperature would then be expected mainly to result in a sharpening of the fluorescence line shape without affecting the anisotropy.

Of the four solvents used in this study, we chose 2-MTHF for a variable temperature study because it forms high-quality clear glasses of carotenoid solutions at cryogenic temperatures,[84] which would be favored to lower the background light scattering that might obscure the weak fluorescence signals anticipated from β-carotene. A fixed excitation wavelength was used, 430 nm, which obtains at room temperature the signal shown in Figure 5b featuring a low anisotropy value, 0.16, in the S_2 and S_1 bands. The absorption and fluorescence spectra were recorded sequentially at a given temperature with the β-carotene sample in 2-MTHF held in a liquid nitrogen cryostat (80−200 K) or in a Peltier-effect temperature controller (258−296 K). We were unable to operate the liquid nitrogen cryostat reliably at higher temperatures than 200 K; no spectra are available over the intermediate 200−258 K range. Figure 7 shows the absorption and fluorescence spectra from β-carotene in 2-MTHF at four temperatures over the 80−258 K range. The four panels present the fluorescence oscillator strength and anisotropy spectra in these solvents in the same manner

https://dx.doi.org/10.1021/acs.jpcb.0c06961
J. Phys. Chem. B 2020, 124, 9029−9046

used above; the full set of wavelength spectra over the 80−296 K range are presented in the Supporting Information.

As the temperature is lowered, the absorption spectrum from β-carotene in 2-MTHF shifts with respect to the room temperature spectrum to lower wavenumbers and develops a sharpened vibronic structure. The line shape function would be expected to narrow as the temperature is lowered, but simulations using the MBO model[65] of the absorption spectra at 80 and 296 K (shown in the Supporting Information) also indicate that the total solvation reorganization energy increases by about 25% at 80 K compared to that at room temperature. This effect can be attributed to constriction of a solvent cavity around the β-carotene chromophore in the ground state as the temperature decreases in the dark prior to illumination. The shift of the absorption spectrum to the red as the temperature is lowered arises from the temperature dependence of the solvent polarizability.[8,16,85,86]

The main result from Figure 7, however, is that the integrated oscillator strength of the fluorescence emission from β-carotene with 430 nm excitation markedly increases as the temperature is lowered due to a new contribution to the emission spectrum from a short-lived spectral "intermediate" along the S_2 to S_1 nonradiative decay pathway. The fluorescence oscillator strength spectra are shown with absolute scaling in Figure 7 to make clear how much stronger the emission is at 80 K; the quantum yield determined from the integrated oscillator strength is 78 times larger at 80 K, 1.5×10^{-4}, than that at room temperature, 2.0×10^{-6}. The emission spectrum over the 80−200 K range (Figure 7a−c) is dominated by a very broad line shape centered roughly at 16,000 cm^{-1} (625 nm), well to the red of that observed from S_2 at higher temperatures (Figure 7d or Figure 5b). As the temperature is increased above 80 K, the fluorescence spectrum maintains its broad lineshape albeit with a small red shift as it decreases in intensity, essentially disappearing above 200 K to reveal the underlying much weaker S_2 and S_1 emission bands characteristic of the high-temperature emission spectrum.

The broad emission lineshape observed over the 80−200 K range very likely corresponds to the formation of a distorted intermediate moving on the out-of-plane potential energy gradient linking the Franck−Condon S_2 state to the CI with the S_1 state (Figure 1). The lineshape is comparable to that determined as the instantaneous species associated difference spectrum (SADS) observed by de Weerd et al.[48] in a global target analysis of their femtosecond pump−continuum probe spectra with β-carotene at room temperature in three solvents. These signals should not be regarded as arising from a conventional intermediate spectroscopic state; the breadth of the fluorescence signals observed in Figure 7a,c (~8000 cm^{-1} at 80 K) would correspond to uncertainty broadening of a state with an infinitesimal lifetime, ~660 as, which would preclude its detection via fluorescence. Thus, the overall breadth of the fluorescence (and SE) signals from β-carotene reflects the integral of narrower lineshapes from molecules moving rapidly on the S_2 out-of-plane gradient over the <150 fs timescale. As the temperature is increased over the 80−258 K range for the example spectra shown in Figure 7, the solvent viscosity (and the resulting friction) decreases over many orders of magnitude.[87] Above 200 K, it is evident that the time spent by a given molecule on the out-of-plane gradient is very short indeed. Very few fluorescence photons are detected during progress to the CI seam with the S_1 state, allowing the high temperature S_2 and S_1 emission bands to be observed.

The high fluorescence anisotropy value detected at 80 K, 0.36 (Figure 7a), indicates that the isoprenoid backbone of β-carotene is still constrained at 80 K to point roughly along the direction of the equilibrium ground state structure even though the emission spectrum reports the presence of a distorted intermediate. This finding strongly suggests that concerted out-of-plane distortions of more than one bond occur along the isoprenoid backbone of β-carotene when large volumes of motion are constrained by the frozen solvent cavity. The "bicycle pedal"[88] and "hula-twist" mechanisms[89] for the retinal PSBs in rhodopsin or bacteriorhodopsin are well-discussed examples of out-of-plane pathways leading to fully photoisomerized structures incorporating torsions of more than one bond along a polyene's length. These structures are termed volume conserving because they can occur from initially all-*trans* configurations despite being confined by the frozen solvent cavity at low temperature.[90] Further, assumption of these structures would not be reported by a large internal rotation of the emission TDM since a large sweep of half of the isoprenoid backbone of β-carotene would not be required as it would for a single-bond distortion.

At higher temperatures, the melting 2-MTHF solvent apparently allows the isoprenoid backbone of β-carotene to lower its conformational potential energy further by relaxing further out-of-plane at a single point along its length. This process results in lower anisotropy values (Figure 7b,c). Figure 8a shows that the minimum anisotropy smoothly decreases over the 80−200 K range to level off at the 0.16 value observed in the S_2 and S_1 emission regions in 2-MTHF at high temperatures. Although the confidence intervals are large and overlap extensively, the anisotropy measured for the S_1 emission exhibits a decreasing trend as the temperature is increased over the 258−296 K range. The lifetime of the S_1 state is ~10 ps,[22,43,76,77] somewhat longer than the 0.5−2 ps timescale associated for vibrational cooling in carotenoids;[84,91] hence, the emission spectrum from S_1 would be expected to be that from an ensemble nearly at thermal equilibrium with the surrounding medium.

An estimate for the effective activation energy barrier that constrains the motion of the S_2 molecules on the out-of-plane gradient leading to the CI seam with the S_1 state is obtained from the slope $-E_a/RT$ of an Arrhenius plot (Figure 8b), plotted in terms of the ratio of nonradiative and radiative rates of decay, $k_{nr}/k_r = \Phi_F^{-1} - 1$.[92,93] Over the 80−200 K range, a linear trend with respect to $1/T$ is observed. The slope corresponds to an activation energy of 140 cm^{-1}, which can be identified as a librational mode of the 2-MTHF solvent medium. Almost exactly the same activation energy was observed in fluorescence anisotropy decay measurements in 2-MTHF with a range of fluorescent probes.[94] To be clear, in this figure, the barrier between the Franck−Condon region and the out-of-plane gradient of the S_2 potential energy surface has been already crossed by the molecules that emit the broad low-temperature fluorescence spectrum shown in Figure 7a−c.

At higher temperatures, the larger slope of the Arrhenius plot determined from the integrated oscillator strength for the high-temperature S_2 and S_1 emission bands indicates an effective activation energy for nonradiative decay, 850 cm^{-1}. This frequency is in the range associated with hydrogen-out-of-plane deformation modes in polyenes.[95,96] The simple dynamical picture used in the thinking here is that effectively

https://dx.doi.org/10.1021/acs.jpcb.0c06961
J. Phys. Chem. B 2020, 124, 9029−9046

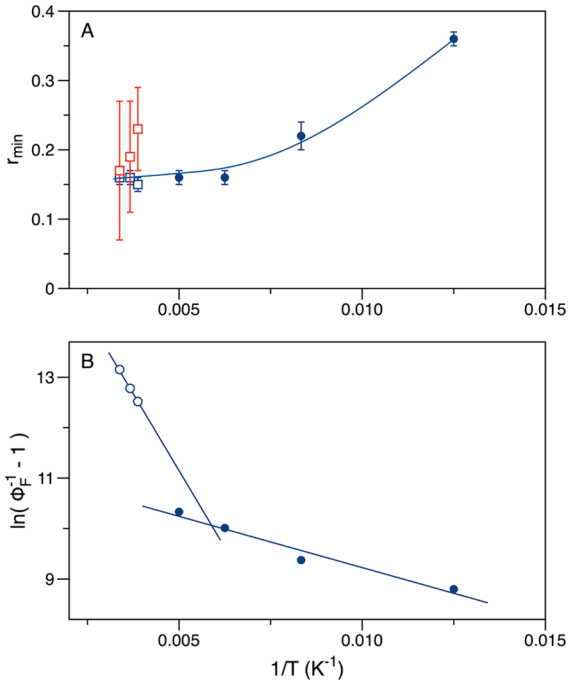

Figure 8. Comparison of the temperature dependences of (a) minimum fluorescence anisotropy and (b) quantum yield of fluorescence for β-carotene in 2-MTHF solvent with excitation at 430 nm. In (a), the trend of the fluorescence anisotropy measured for the emission from the spectral intermediate (Figure 7a–c) observed over the 80–200 K range (solid blue circles) is extended to compare with the anisotropy measured over the 258–296 K range for the S_2 (blue open squares) and S_1 (red open squares) bands. Error bars report the +/− standard deviations over the sampled spectral regions. In the Arrhenius-style plot shown in (b), E_a = 140 ± 20 cm^{-1} for 80–200 K (solid blue circles) and E_a = 850 ± 5 cm^{-1} for 258–296 K (open blue circles).

an exchange of vibrational quanta with the surroundings promotes the passage of the β-carotene molecules from the S_2 state to the S_1 state through a CI seam between the two potential energy surfaces, so the quanta of the key promoting modes contributes to the activation energies.

The coupling of the temperature dependence of the fluorescence quantum yield and anisotropy observed here for β-carotene in 2-MTHF has not been reported previously, to our knowledge, but Andersson et al.[92] observed a comparable temperature dependence for the quantum yield of fluorescence from the triene analog of β-carotene, mini-3. The mini-carotenes exhibit a fluorescence spectrum with a more pronounced "dual" character, with both bands originating from the S_2 and S_1 states apparent.[97] The shortest of these, mini-3, having only a single/double bond backbone between the two β-cyclohexane rings, absorbs in the 250 nm region of the UV and emits in the 360 nm region. The fluorescence quantum yield of mini-3 was observed to follow an Arrhenius dependence with an activation energy of 610 cm^{-1}; over the 77–110 K temperature range, the quantum yield decreases from 0.61 to 0.04. Andersson et al. discuss this trend in terms of a nonradiative decay mechanism promoted by out-of-plane torsional motions. The fluorescence anisotropy measured at 77 K is high, 0.39, but unfortunately no measurements of the anisotropy at higher temperatures were reported, most likely because the fluorescence quantum yield decreases to very low values in liquid media, rendering it effectively "nonfluorescent".[92] In mini-3, the activation energy barrier for access from the Franck–Condon region of the S_2 potential surface to the out-of-plane gradient (as in Figure 1) would be expected to be small or nonexistent compared to that in β-carotene. In comparison, as noted above, the temperature dependence noted for β-carotene in Figures 7 and 8 was observed with excitation at 430 nm, well above the wavenumber of the 0–0 transition.

DFT Calculations. To explore how internal out-of-plane structural deformations of the isoprenoid backbone of β-carotene in the S_2 state might cause the emission TDM to rotate, producing the experimentally observed low minimum fluorescence anisotropies (Table 1), we computed the electronic structures of a set of torsionally distorted conformers starting from the all-*trans* structure. As the simplest case, we consider here a single torsional coordinate for the initial excited state relaxation away from the Franck–Condon region of the S_2 potential energy surface. Of course, the possibility that rotations of more than one coordinate of the isoprenoid backbone contribute to the observed rotation of the TDM should not be dismissed arbitrarily. As noted above, concerted or sequential torsions of more than one C–C bond have been discussed, in particular for the photochemistry of retinal PSBs in rhodopsin and bacteriorhodopsin.[90] Further, calculations by Hynes and co-workers[98] on retinal PSB models indicate that the torsional and pyramidal coordinates are strongly coupled; the out-of-plane distortions observed in β-carotene would very likely involve simultaneous displacements along both coordinates.

Potential energy surface scans in the electronic ground state, S_0, were conducted with respect to torsions of each of the labeled bonds numbered in Figure 9a, with the C–C=C–C dihedral angle being varied from 180° for the nominally planar, all-*trans* structure to 90°. This procedure allows a smooth relaxation of the internal coordinates to accompany the fixed torsional distortion. The computed transition density isosurfaces and the $S_0 \rightarrow S_2$ absorption TDM vectors for the particular example of rotation around the C_{15}–$C_{15'}$ double bond are shown in Figure 9b. The colored isosurfaces show how the π-electron density increases or decreases upon optical excitation. The TDM vectors are referenced in each conformation with respect to the center of mass. Figure 9c summarizes how the orientation of the TDM depends on which C–C bond in the isoprenoid backbone is twisted to assume a 90° conformation. The rotation angle is determined relative to the orientation of the TDM for the all-*trans* configuration. This angle would be expected to be comparable to that for the vertical fluorescence emission transition from a distorted S_2 structure to the ground state. Twisting of bonds 14–15, 15–15′, and 15′–14′ to the 90° conformation rotates the TDM by 28–35°, with the largest rotation arising from twisting the central C_{15}–$C_{15'}$ bond.

The results shown in Figure 9c for rotations of the absorption TDM due to torsions of the isoprenoid backbone of β-carotene in the ground state are recapitulated by relaxed scans of the S_2 potential energy surface of a truncated version of β-carotene in which the β-ionone rings have been replaced by hydrogen atoms (Figure 9a). This truncation lessens the time and considerable expense required for excited-state optimizations; the π-electron density is mostly resident on this section of the β-carotene structure. Figure 9d compares the calculated rotations for the $S_0 \rightarrow S_2$ absorption and $S_2 \rightarrow S_0$ emission TDMs with respect to torsions of the C_{15}–$C_{15'}$ bond

https://dx.doi.org/10.1021/acs.jpcb.0c06961
J. Phys. Chem. B 2020, 124, 9029–9046

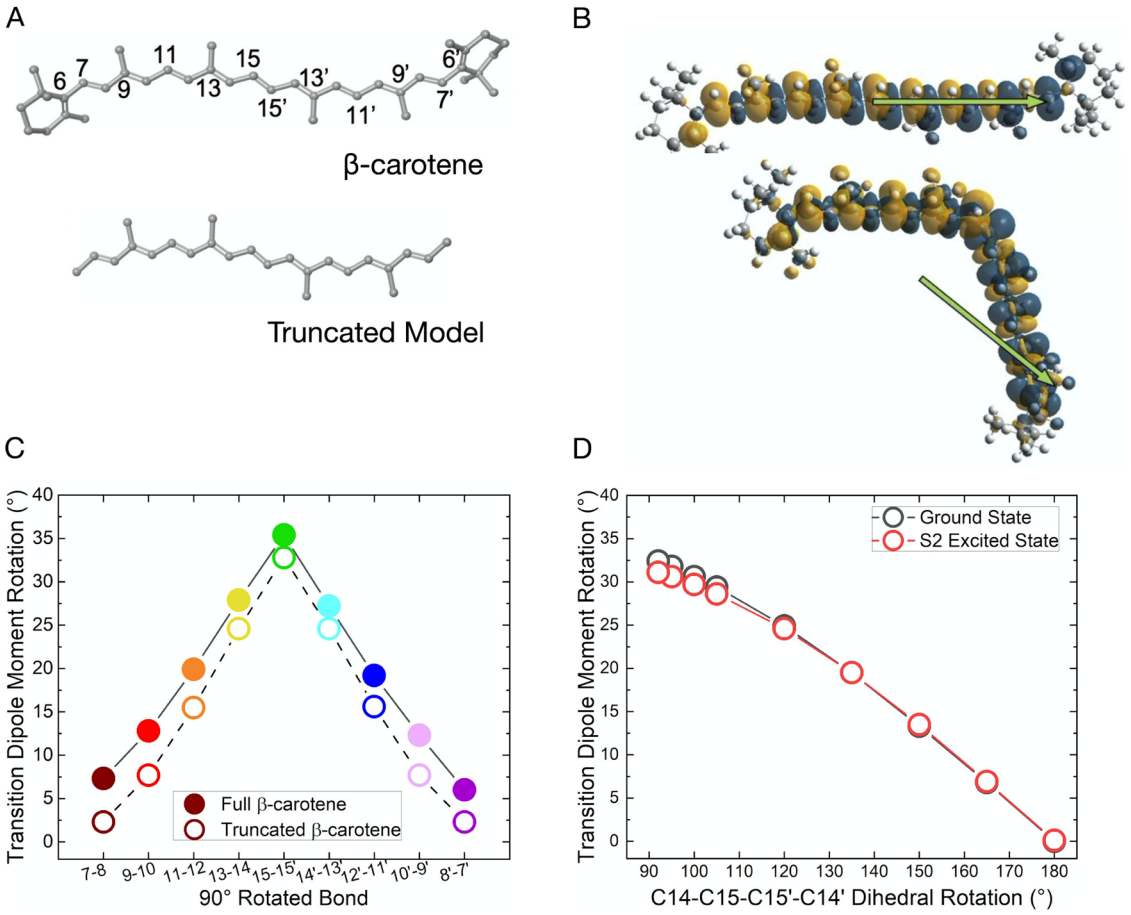

Figure 9. (a) Minimum energy structure of *β*-carotene and of a truncated model, with a numbering scheme indicated (as also used in Scheme 1) for the carbon atoms in the isoprenoid backbone. (b) Optical transition densities for the $S_0 \rightarrow S_2$ absorption transition for the all-*trans* structure and for the $C_{15}-C_{15'}$ 90°-twisted structure. Orange/blue orbital colors denote an instantaneous gain or loss of electron density, respectively, upon excitation. Green arrows indicate the direction of the TDM with the vector origins drawn at the center of mass. (c) Calculated TDM rotations with respect to the all-*trans* structure as a function of the choice of the bond undergoing a 90° torsion for the $S_0 \rightarrow S_2$ absorption TDM, the latter for the truncated model. (d) Calculated rotations for the $S_0 \rightarrow S_2$ absorption and $S_2 \rightarrow S_0$ emission TDMs with respect to the torsions of the $C_{15}-C_{15'}$ bond of *β*-carotene, the latter for the truncated model.

for the truncated model. The TDM rotations were found to agree within 2°. This agreement justifies the use of ground state conformers for the TDM rotation analysis for the full *β*-carotene structure (Figure 9c). The close agreement between these two calculations demonstrates that 90° torsional distortions of a single C−C bond near the center of the isoprenoid backbone are remarkably consistent with the 39° TDM rotations determined by the fluorescence anisotropy values of 0.16 for the S_2 band in the polar solvents, chloroform and 2-MTHF (Table 1). The barrier for torsions would be expected to be the lowest near the center of the isoprenoid backbone, where the BLA amplitude is the smallest along the chain.[20]

It is important to clearly state the assumptions we are making to model the hypothesized torsional conformations. The purpose of the scan of the torsional angles on the S_0 and S_2 surfaces, the latter for the truncated model, is strictly to make a correlation between the structure and the direction of the vertical transition dipole moment (TDM) for transitions between the two surfaces. This work is intended to extend the general conclusion[16,74] that the transition dipole moments of linear polyenes point down the isoprenoid backbone. To our knowledge, there have not been any reports of electronic structure calculations of the TDM directions in twisted conformers or even in *cis* configurations. The structures at each torsional angle should be considered local minima because the energy was minimized at each stated torsional conformation, primarily to avoid steric clashes, but a global minimum energy path was not sought given that we held only one torsion fixed during the energy minimization. Further, we have not attempted calculations of the TDM direction in the S_1 state because it is well known that TDDFT methods should not be used to model states involving a large component of double excitations. There is no reason to suggest, however, that the S_1 state's TDM direction should point in a different direction from that determined for the S_0 or S_2 states.

A physical explanation for the larger rotations of the TDM observed in the nonpolar solvents, 48−50°, requires the displacement of an additional coordinate of the isoprenoid backbone of *β*-carotene during the fluorescence emission timescale. Of particular interest is the possibility that a pyramidal distortion converts the diradical electron configuration of a twisted bond to the lone-pair configuration consistent with a full ICT.[50,51] The pyramidal structure corresponds to a candidate for a CI of the S_2 state with the S_1 state. Although determination of a true CI on the S_2 surface is beyond the scope of the present work (and beyond the capabilities of TDDFT for such a large system), we

https://dx.doi.org/10.1021/acs.jpcb.0c06961
J. Phys. Chem. B 2020, 124, 9029−9046

constructed an ad hoc model for the β-carotene CI structure using a template constructed with the internal coordinates of ethylene at the CI determined by Minezawa and Gordon[99] using spin-flip TDDFT. In particular, the ethylene CI structure was superimposed with our 90° rotated structure, as obtained via the relaxed scan discussed above. After this, the four dihedral angles of the $C_{15}-C_{15'}$ bond were manually adjusted to visually maximize the overlap between the $C_{15}-C_{15'}$ adjacent atoms and those of the ethylene CI. The structure was then relaxed in the ground state but keeping the dihedral angles of the $C_{15}-C_{15'}$ bond fixed to minimize steric interactions.

Figure 10 shows the superposition of three relevant conformations: the all-*trans* structure, the 90° rotated structure

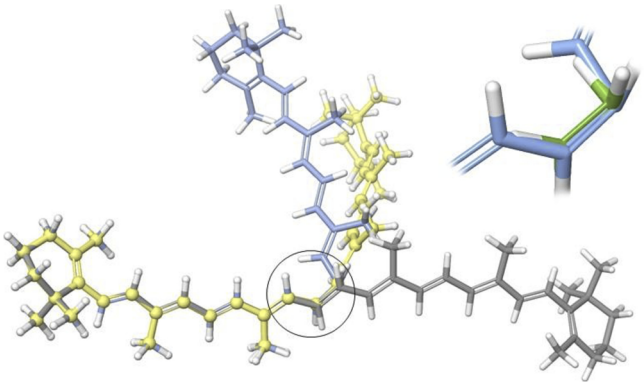

Figure 10. Modeled structures representing the Franck–Condon S_2 structure (gray), the 90° twisted conformer (yellow), and a conformer with a pyramidal distortion (light blue). The inset is a zoomed-in view of the circled region, which shows the modeled β-carotene pyramidal structure superimposed with the pyramidal structure of the CI of ethylene (green).[99]

used in Figure 9b, which gives rise to a 35° rotation of the TDM, and the pyramidal structure resembling the ethylene CI. For the latter structure, the calculated TDM rotation is 47°. This result is remarkably similar to the 48–50° rotation angle observed in the fluorescence anisotropy measurements for the S_1 state in the nonpolar solvents (Table 1).

Figure 11 shows how the emission TDM vectors for the Franck–Condon S_2 state and those of the 90° twisted and

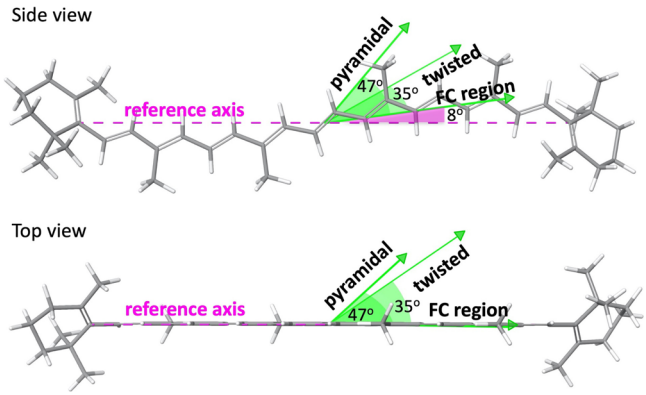

Figure 11. Orientations of the emission TDM vectors for the Franck–Condon S_2 state and those of the 90° twisted and pyramidal S_2 conformations with respect to the ground-state structure of β-carotene. The reference axis is the $C_6-C_{6'}$ vector.

pyramidal S_2 conformations are oriented with respect to the molecular frame of the ground-state structure of β-carotene. The ground-state all-*trans* structure is shown in two orientations, with the point-of-view directed in the plane and from above. The TDM vectors are drawn with their origins placed at the center-of-mass, which coincides with the midpoint $C_{15}-C_{15'}$ bond.

The TDM for the Franck–Condon S_2 state is rotated by 8° with respect to the molecular frame axis, which is chosen here as the vector connecting the C_6 and $C_{6'}$ atoms on the opposite ends of the isoprenoid backbone. In comparison, Birge et al.[53] obtained an estimate of 15° for the orientation of the TDM compared to the molecular frame axis for a conjugated polyene with $N = 11$ conjugated polyene double bonds with the methyl groups included along the backbone and 12.6° if the methyl groups were not included. The effective conjugation length for β-carotene is shorter than this, but similar values were obtained for $N = 8–15$. Similarly, Dolan et al.[54] used linear dichroism measurements in squeezed polyacrylamide gels to determine that the absorption TDM is rotated 9.1° from the molecular frame axis in the "corkscrew" ground state conformation of rhodopsin glucoside in LH2 from *Rhodopseudomonas acidophila* strain 10050.

Table 2 compares the permanent dipole moments in the ground and S_2 states and the rotations of the TDMs for the

Table 2. Permanent Dipole Moments and TDM Rotations for the Calculated β-Carotene S_2 Structures (Figure 10)

structure	dipole moment (D)	TDM rotation[a]
S_0	0.1	
S_2 (Franck–Condon)	0.2	0° (reference)
S_2 90-twisted	1.6	35°
S_2 pyramidal	8.3	47°

[a]Deviation angle from the direction of the vertical S_2 TDM.

three structures shown in Figure 10. Photoexcitation to the S_2 state results in only a small increase in the nonzero permanent dipole moment exhibited by the ground-state structure, which is not perfectly C_2 symmetric. The 90° twisted structure has a larger dipole moment, 1.6 D, which implies a significant polar character. A substantially larger dipole moment is determined for the pyramidal structure, 8.3 D, indicating ICT across the $C_{15}-C_{15'}$ bond and delocalization on either side of it. These results are consistent with the suggestion that the evolution on the S_2 surface should be accompanied by a large increase in the solvent friction as the structure nears the CI with the S_1 state.

DISCUSSION & CONCLUSIONS

The results presented above suggest a new picture for the photophysical and photochemical properties of carotenoids arising from the optical preparation of the bright S_2 state. As demonstrated here with β-carotene in several aprotic solvents, fluorescence emission is observed from two distinct groups of excited-state molecules depending on the excitation wavelength. A fraction is retained by a low activation barrier near the Franck–Condon geometry (Figure 1); these molecules are optically prepared by absorption transitions near the 0–0 transition. The fluorescence spectrum from these S_2 state molecules is roughly mirror symmetric with respect to the absorption spectrum, and the fluorescence anisotropy is at least 0.35, near the 0.4 value expected for molecules retaining the essentially planar all-*trans* structure photoselected from the

https://dx.doi.org/10.1021/acs.jpcb.0c06961
J. Phys. Chem. B 2020, 124, 9029–9046

ground-state ensemble. An example of a fluorescence spectrum predominantly from these molecules is that observed from β-carotene in hexane with 490 nm excitation (Figures 2a and 3a).

As the excitation wavelength is tuned to the blue over the ∼3000 cm^{-1} range spanned in the vibronic structure from the 0−0 transition to the 0−3 transition, an increasing fraction of S_2 state molecules are able to pass over an activation barrier dividing the planar and out-of-plane distorted regions of the S_2 potential energy surface. This part of the excited-state ensemble contributes at high temperatures to a broadening of the red tail of the S_2 spectrum and to a more prominent and blue-shifted S_1 emission band compared to that observed upon nonradiative decay from the planar molecules retained by the barrier. In carbon disulfide, chloroform, and 2-MTHF, the fraction of S_2 molecules crossing over the activation barrier is significant even at the longest excitation wavelengths used in the present experiments, given the observation of fluorescence anisotropies <0.3 in the S_2 emission band (Table 1). This finding suggests that the barrier height is significantly lower in these solvents than in hexane.

The work presented here provides the key connection that the near-IR portion of the emission from S_2 and the enhanced emission from S_1 observed with blue excitation has a low fluorescence anisotropy. This finding indicates that passage over the activation barrier is followed by evolution on a steep gradient on the S_2 state potential energy surface with respect to the out-of-plane coordinates of the isoprenoid backbone (Figure 1), producing emission that is progressively red shifted from the mirror-symmetric S_2 emission. Over the 80−200 K range, we observed a broad emission band with an enhanced emission quantum yield and a temperature-dependent anisotropy that arises from a dynamic intermediate, perhaps S_x or its successor evolving on the out-of-plane gradient. Progress along the out-of-plane coordinates in the S_2 state results in rotation of the emission TDM and quenching of the initially strong emission oscillator strength. Further, electronic structure calculations (Table 2) indicate that an enhanced permanent dipole moment develops due to ICT as the out-of-plane coordinates advance, especially with pyramidalization. The ICT character imparts some solvent sensitivity to the barrier height because the gradient region of the S_2 potential energy surface is increasingly stabilized in polar or polarizable solvents. Despite being nonpolar, carbon disulfide may have a significant impact on the barrier height in β-carotene because of first solvation shell interactions by the highly polarizable sulfur atoms.

The preceding description of the fluorescence emission from β-carotene is unconventional because it discusses the emission line shape as being *dynamic*, reporting fast, large amplitude motions on the S_2 state potential energy surface. As determined in the present experiments with continuous excitation, the recorded fluorescence line shape is the sum of the instantaneous, time-resolved line shapes emitted by the evolving excited-state ensemble. This situation is made especially obvious in β-carotene for the barrier-crossing molecules because the structural evolution is ultrafast compared to the vibrational relaxation time. In this dynamic picture, the fluorescence line shape, quantum yield, and anisotropy are very sensitive probes of changes in the molecular properties of a chromophore during the emission process.

Several of these ideas have precedence in the work by Kochendoerfer and Mathies[82] on the fluorescence of the retinal PSBs in rhodopsin and isorhodopsin.[82,100] As background on this point, recall that the ordering of the lowest two electronic states for the retinal PSBs is inverted compared to that for carotenoids, with the bright S_1 ($^1B_u^+$) state lying below the dark S_2 ($^1A_g^-$) state.[101] The quantum yield of fluorescence from S_1 is very small due to fast nonradiative recovery to the ground state and photochemistry in a significant fraction of events in the proteins, less so in solution. The potential energy surface of the S_1 state is usually considered barrierless for 11-*cis*-retinal in rhodopsin and isorhodopsin.[102,103] In contrast, a low barrier may precede the torsional gradient on the excited state potential energy surface for all-*trans*-retinal in bacteriorhodopsin.[104,105]

Kochendoerfer and Mathies[82] observed that the maximum of the fluorescence spectrum from retinal in rhodopsin and isorhodopsin tracks the excitation wavelength as it is tuned to shorter wavelengths. At the same time, however, it is notable that the fluorescence line shape broadens considerably into the near-IR. These behaviors are very similar to those reported here for the fluorescence of β-carotene. By tuning to shorter wavelengths, the energy of the Franck−Condon structure is increased on the excited-state potential energy surface. Given the present paper's context, the increased breadth of the fluorescence spectrum observed by Kochendoerfer and Mathies with excitation at blue wavelengths is probably consistent with the presence of a low barrier on the retinal excited-state potential energy surface. Although measurements of the fluorescence anisotropy were not reported by Kochendoerfer and Mathies, low fluorescence anisotropies were observed with excitation at shorter wavelengths in early studies of fluorescence in rhodopsin and bacteriorhodopsin.[106,107] It is also notable that a low anisotropy was observed in the SE signals detected in femtosecond pump−probe anisotropy measurements in bacteriorhodopsin by Haran et al.[108]

The present work develops for the first time, however, that the fluorescence anisotropy can provide information on the structure of the isoprenoid backbone of a carotenoid prior to and after nonradiative passage from the S_2 state to the S_1 state. As listed in Table 1, the minimum fluorescence anisotropy measured in the S_2 and S_1 bands for β-carotene with 430 nm excitation in the polar solvents, chloroform and 2-MTHF, is fully consistent with that calculated for a 90° twist of one of the carbon−carbon bonds in the middle of the isoprenoid backbone (Figure 9). This finding indicates that nonradiative decay from S_2 to S_1 occurs when the isoprenoid backbone is significantly distorted along the coupled torsional and pyramidal coordinates but very likely not at the minimum along the S_2 gradient. The S_2 and S_1 emission bands overlap extensively; an unambiguous determination of the fluorescence anisotropy achieved at the CI seam is not possible. But it is clear that the S_1 emission TDM is rotated even further in the nonpolar solvents, to a rotation of almost 50°. This observation is consistent with the rotation of the emission TDM calculated for a pyramidalized, zwitterionic structure. One explanation for this solvent effect is that solvent friction arising from the developing ICT character significantly slows the progress made on the out-of-plane gradient in the S_2 state. Note that the S_1 state apparently retains a distorted conformation over its 10 ps fluorescence lifetime, which is significantly longer than that expected for vibrational relaxation and thermal equilibration on the S_1 surface.

https://dx.doi.org/10.1021/acs.jpcb.0c06961
J. Phys. Chem. B 2020, 124, 9029−9046

This discussion indicates that a multicoordinate anharmonic picture is required even to understand qualitatively the excitation wavelength-dependent S_1 emission observed from β-carotene in the four solvents. The weaker and red-shifted S_1 emission band arising from photoexcited molecules retained by the activation barrier originates from a minimum on the S_1 potential energy surface in the Franck−Condon region, which is not displaced very much with respect to the out-of-plane coordinates of the isoprenoid backbone. In comparison, a significantly stronger and somewhat blue-shifted S_1 emission band is observed from the molecules that pass over the activation barrier. This emission arises from a distinct minimum on the S_1 potential energy surface with a significant displacement from the Franck−Condon structure along the out-of-plane coordinates. The enhanced strength of the emission from the distorted S_1 minimum can be attributed to an enhanced intensity borrowing from the S_2 state that accompanies out-of-plane distortions of the isoprenoid backbone. Note that the apparent enhancement of the depth of the vibronic structure in the S_1 emission suggests the possibility that this minimum has a larger displacement along the BLA coordinates than the Franck−Condon minimum.

The discussion of solvent friction brings up the important question of how a carotenoid would be expected to act when bound in a nonpolar site in a photosynthetic light-harvesting protein or a reaction center. As noted above, all-*trans* configurations of carotenoids in proteins usually exhibit distorted conformations, which would already favor out-of-plane distortions following the vertical optical transition from the ground state. The present study of the low-temperature fluorescence properties of β-carotene now makes it clear that large amplitude out-of-plane motions are possible even when the motions of the isoprenoid backbone are strongly hindered by the surrounding medium, as they perhaps would be in a protein. The finding that the dynamic intermediate observed over the 80−200 K range exhibits a decreasing fluorescence anisotropy as the solvent melts is proof, however, that the isoprenoid backbone can be further stabilized by undergoing a larger volume of rotation, principally with respect to one of the carbon−carbon bonds near the center of the chain.

The conclusion that out-of-plane distorted S_2 structures can be formed despite steric hindrance from the surrounding medium is fully consistent with the recent studies by Geiger, Borhan, and co-workers[109,110] on engineered model retinal PSB-binding proteins, where full photoisomerization, not just conformational distortion, is observed even in protein crystals. In these studies, the X-ray crystal structures indicate that the TDM of the photochemical product species would be restricted to point along the binding site's principal axis. A similar conclusion would be made on the basis of Warshel's early analysis of the photoisomerization mechanism in rhodopsin, where the "bicycle pedal" isomerization mechanism is proposed.[88]

Part of the motivation behind the present study of β-carotene has been our interest in understanding the spectroscopy of ketocarotenoids, especially those that function in light harvesting and photoprotection in photosynthetic organisms.[111,112] The presence of a carbonyl substituent on the isoprenoid backbone would be expected to have an especially large impact on the dynamics on the S_2 and S_1 surfaces due to its electron-withdrawing character, which would enhance the permanent dipole moment due to ICT and increase the solvent friction. In previous work from this laboratory, we suggested that evolution from the Franck−Condon S_2 state of peridinin to the S_x state involves twisting and pyramidal distortions of the isoprenoid backbone, both in solution and in the peridinin−chlorophyll protein.[44,113] As noted above, the lifetime of the S_x state of peridinin is proposed to be significantly longer than that for carotenoids lacking carbonyl substitution, like β-carotene, because passage on the out-of-plane gradient to the CI seam to the S_1 state would be significantly slowed by solvent friction.[43−45]

More connected to the present work, however, are the observations we made previously of the fluorescence properties of the ketocarotenoids 3′-hydroxyechinenone and canthaxanthin in the orange carotenoid protein. These two ketocarotenoids exhibit broad, mirror-asymmetric fluorescence spectra assigned to the S_2 state with many of the line-shape properties reported here for β-carotene.[56] The carbonyl substituents are located on one or both of the β-ionone end rings, respectively, where they would not be especially strongly coupled to the π-electron density because the rings are canted out of plane with respect to the isoprenoid backbone. These were the first fluorescence studies performed in this laboratory on carotenoids, and we did not examine the S_1 emission bands at that time. The quantum yields of emission from S_2 for 3′-hydroxyechinenone and canthaxanthin in OCP, however, were measured to be several orders of magnitude larger than that observed here for β-carotene. We suggested that this finding might be explained if the ketocarotenoid-binding site in OCP hinders the out-of-plane distortions that promote nonradiative decay to the S_1 state especially owing to hydrogen-bonding interactions between the carbonyls on the β-ionone end rings and the surrounding protein. This suggestion is in line with the present finding that much larger quantum yields of emission are observed from the β-carotene dynamic intermediate at low temperature over the 80−200 K region.

As a concluding comment, the extent to which the ketocarotenoids can move conformationally out of plane of the isoprenoid backbone after photoexcitation to the S_2 state when bound in a protein site is not well understood at present. In future work, it will clearly be of considerable interest to determine how the fluorescence anisotropy in the near-IR emission bands of the ketocarotenoids is impacted by the presence of the carbonyl substituent. Knowledge of the direction of the emission TDM will allow a better understanding of the evolution of the structure as relaxation occurs on the S_2 potential energy surface and of the nature of the mixing with the S_1 state.

■ ASSOCIATED CONTENT

Supporting Information

The Supporting Information is available free of charge at https://pubs.acs.org/doi/10.1021/acs.jpcb.0c06961.

Materials and Methods: sample handling and details of the fluorescence spectroscopy methods; Appendices: fluorescence lineshape and anisotropy wavelength spectra from β-carotene in the four aprotic solvents as a function of excitation wavelength; multimode Brownian oscillator models (PDF)

https://dx.doi.org/10.1021/acs.jpcb.0c06961
J. Phys. Chem. B 2020, 124, 9029−9046

AUTHOR INFORMATION

Corresponding Author

Warren F. Beck − *Department of Chemistry, Michigan State University, East Lansing, Michigan 48824, United States;* orcid.org/0000-0002-7491-0264; Email: beckw@msu.edu

Authors

J. K. Gurchiek − *Department of Chemistry, Michigan State University, East Lansing, Michigan 48824, United States*

Justin B. Rose − *Department of Chemistry, Michigan State University, East Lansing, Michigan 48824, United States*

Matthew J. Guberman-Pfeffer − *Department of Chemistry, University of Connecticut, Storrs, Connecticut 06268-1712, United States*

Ryan W. Tilluck − *Department of Chemistry, Michigan State University, East Lansing, Michigan 48824, United States*

Soumen Ghosh − *Department of Physics, Politecnico di Milano, Milan, Lombardy 20133, Italy;* orcid.org/0000-0002-3323-1724

José A. Gascón − *Department of Chemistry, University of Connecticut, Storrs, Connecticut 06268-1712, United States;* orcid.org/0000-0002-4176-9030

Complete contact information is available at: https://pubs.acs.org/10.1021/acs.jpcb.0c06961

Notes

The authors declare no competing financial interest.

ACKNOWLEDGMENTS

Experimental work in this project in the laboratory of W.F.B. was principally supported by the Photosynthetic Systems program of the Chemical Sciences, Geosciences and Biosciences Division, Office of Basic Energy Sciences, Office of Science, U.S. Department of Energy under award DE-SC0010847. Work on electronic structure in the laboratories of J.G. and theoretical analysis of the experimental results in the laboratory of W.F.B. was supported by a collaborative research grant from the Chemistry of Life Sciences program of the U.S. National Science Foundation, awards CHE-1904700 and CHE-1904655, respectively. J.A.G. acknowledges the support from NSF (CHE-1404998). M.J.G-P. was supported by a National Science Foundation Graduate Fellowship (DGE-1247393). Additionally, we would like to thank Professor Harry A. Frank and Amy LaFountain (University of Connecticut) for the generous gift of the purified β-carotene samples employed in this study and for several useful suggestions during the experiments and during preparation of the manuscript.

REFERENCES

(1) Polívka, T.; Sundström, V. Ultrafast Dynamics of Carotenoid Excited States—from Solution to Natural and Artificial Systems. *Chem. Rev.* **2004**, *104*, 2021−2072.

(2) Polívka, T.; Frank, H. A. Molecular Factors Controlling Photosynthetic Light Harvesting by Carotenoids. *Acc. Chem. Res.* **2010**, *43*, 1125−1134.

(3) Polívka, T.; Sundström, V. Dark Excited States of Carotenoids: Consensus and Controversy. *Chem. Phys. Lett.* **2009**, *477*, 1−11.

(4) Beck, W. F.; Bishop, M. M.; Roscioli, J. D.; Ghosh, S.; Frank, H. A. Excited State Conformational Dynamics in Carotenoids: Dark Intermediates and Excitation Energy Transfer. *Arch. Biochem. Biophys.* **2015**, *572*, 175−183.

(5) Hashimoto, H.; Uragami, C.; Yukihira, N.; Gardiner, A. T.; Cogdell, R. J. Understanding/unravelling Carotenoid Excited Singlet States. *J. R. Soc., Interface* **2018**, *15*, 20180026.

(6) Tully, J. C. Perspective: Nonadiabatic Dynamics Theory. *J. Chem. Phys.* **2012**, *137*, 22A301.

(7) Levine, B. G. Nonadiabatic Dynamics of *cis*−*trans* Photoisomerization—a First Principles Study. Ph. D. dissertation, University of Illinois at Urbana-Champagne: Urbana, Illinois, 2007.

(8) Gillbro, T.; Cogdell, R. J. Carotenoid Fluorescence. *Chem. Phys. Lett.* **1989**, *158*, 312−316.

(9) Demchenko, A. P.; Tomin, V. I.; Chou, P.-T. Breaking the Kasha Rule for More Efficient Photochemistry. *Chem. Rev.* **2017**, *117*, 13353−13381.

(10) Christensen, R. L. The Electronic States of Carotenoids. In *The Photochemistry of Carotenoids*; Frank, H. A.; Young, A. J.; Britton, G.; Cogdell, R. J., Eds.; Springer Netherlands: Dordrecht, 1999; pp. 137−159.

(11) Frank, H. A.; Christensen, R. L. Excited Electronic States, Photochemistry and Photophysics of Carotenoids. In *The Carotenoids*; Britton, G.; Liaaen-Jensen, S.; Pfander, H., Eds.; Birkhauser Verlag: Basel, 2008; pp. 167−188.

(12) Schulten, K.; Karplus, M. On the Origin of a Low-Lying Forbidden Transition in Polyenes and Related Molecules. *Chem. Phys. Lett.* **1972**, *14*, 305−309.

(13) Hudson, B.; Kohler, B. Linear Polyene Electronic Structure and Spectroscopy. *Annu. Rev. Phys. Chem.* **1974**, *25*, 437−460.

(14) Holtom, G. R.; McClain, W. M. Two-Photon Excitation Spectra of the Low Energy Excited States of Diphenylhexatriene and Diphenyloctatetraene. *Chem. Phys. Lett.* **1976**, *44*, 436−439.

(15) Hudson, B. S.; Kohler, B. E. A Low-Lying Weak Transition in the Polyene α,ω-Diphenyloctatetraene. *Chem. Phys. Lett.* **1972**, *14*, 299−304.

(16) Hudson, B. S.; Kohler, B. E.; Schulten, K. Linear Polyene Electronic Structure and Potential Surfaces. In *Excited States*; Lim, E. C., Ed.; Elsevier, 1982; Vol. *6*, pp. 1−95.

(17) Nagae, H.; Kuki, M.; Zhang, J.-P.; Sashima, T.; Mukai, Y.; Koyama, Y. Vibronic Coupling through the In-Phase, C=C Stretching Mode Plays a Major Role in the $2A_g^-$ to $1A_g^-$ Internal Conversion of All-*trans*-β-Carotene. *J. Phys. Chem. A* **2000**, *104*, 4155−4166.

(18) Yarkony, D. R. Conical Intersections: Diabolical and Often Misunderstood. *Acc. Chem. Res.* **1998**, *31*, 511−518.

(19) Levine, B. G.; Martínez, T. J. Isomerization through Conical Intersections. *Annu. Rev. Phys. Chem.* **2007**, *58*, 613−634.

(20) Fuß, W.; Haas, Y.; Zilberg, S. Twin States and Conical Intersections in Linear Polyenes. *Chem. Phys.* **2000**, *259*, 273−295.

(21) Sampedro Ruiz, D.; Cembran, A.; Garavelli, M.; Olivucci, M.; Fuß, W. Structure of the Conical Intersections Driving the *cis*−*trans* Photoisomerization of Conjugated Molecules. *Photochem. Photobiol.* **2002**, *76*, 622−633.

(22) Wasielewski, M. R.; Kispert, L. D. Direct Measurement of the Lowest Excited Singlet State Lifetime of All-Trans-β-Carotene and Related Carotenoids. *Chem. Phys. Lett.* **1986**, *128*, 238−243.

(23) Frank, H. A.; Bautista, J. A.; Josue, J.; Pendon, Z.; Hiller, R. G.; Sharples, F. P.; Gosztola, D.; Wasielewski, M. R. Effect of the Solvent Environment on the Spectroscopic Properties and Dynamics of the Lowest Excited States of Carotenoids. *J. Phys. Chem. B* **2000**, *104*, 4569−4577.

(24) Warshel, A.; Karplus, M. Calculation of $\pi\pi^*$ Excited State Conformations and Vibronic Structure of Retinal and Related Molecules. *J. Am. Chem. Soc.* **1974**, *96*, 5677−5689.

(25) Hemley, R.; Kohler, B. E. Electronic Structure of Polyenes Related to the Visual Chromophore. A Simple Model for the Observed Band Shapes. *Biophys. J.* **1977**, *20*, 377−382.

(26) Requena, A.; Cerón-Carrasco, J. P.; Bastida, A.; Zúñiga, J.; Miguel, B. A Density Functional Theory Study of the Structure and Vibrational Spectra of β-Carotene, Capsanthin, and Capsorubin. *J. Phys. Chem. A* **2008**, *112*, 4815−4825.

(27) Fiedor, L.; Pilch, M. Side Methyl Groups Control the Conformation and Contribute to Symmetry Breaking of Isoprenoid Chromophores. *Angew. Chem. Int. Ed. Engl.* **2018**, *57*, 6501−6506.
(28) Andersson, P. O.; Takaichi, S.; Cogdell, R. J.; Gillbro, T. Photophysical Characterization of Natural *cis*-Carotenoids. *Photochem. Photobiol.* **2001**, *74*, 549−557.
(29) Fiedor, L.; Heriyanto; Fiedor, J.; Pilch, M. Effects of Molecular Symmetry on the Electronic Transitions in Carotenoids. *J. Phys. Chem. Lett.* **2016**, *7*, 1821−1829.
(30) Wei, T.; Balevičius, V.; Polívka, T.; Ruban, A. V.; Duffy, C. D. P. How Carotenoid Distortions May Determine Optical Properties: Lessons from the Orange Carotenoid Protein. *Phys. Chem. Chem. Phys.* **2019**, *21*, 23187−23197.
(31) Kuhlman, T. S.; Glover, W. J.; Mori, T.; Møller, K. B.; Martínez, T. J. Between Ethylene and Polyenes−the Non-Adiabatic Dynamics of *cis*-Dienes. *Faraday Discuss.* **2012**, *157*, 193−212. discussion 243−284
(32) Levine, B. G.; Martínez, T. J. Ab Initio Multiple Spawning Dynamics of Excited Butadiene: Role of Charge Transfer. *J. Phys. Chem. A* **2009**, *113*, 12815−12824.
(33) Shu, Y.; Truhlar, D. G. Doubly Excited Character or Static Correlation of the Reference State in the Controversial 2^1A_g State of Trans-Butadiene? *J. Am. Chem. Soc.* **2017**, *139*, 13770−13778.
(34) Glover, W. J.; Mori, T.; Schuurman, M. S.; Boguslavskiy, A. E.; Schalk, O.; Stolow, A.; Martínez, T. J. Excited State Non-Adiabatic Dynamics of the Smallest Polyene, *trans* 1,3-Butadiene. II. Ab Initio Multiple Spawning Simulations. *J. Chem. Phys.* **2018**, *148*, 164303.
(35) Andreussi, O.; Knecht, S.; Marian, C. M.; Kongsted, J.; Mennucci, B. Carotenoids and Light-Harvesting: From DFT/MRCI to the Tamm−Dancoff Approximation. *J. Chem. Theory Comput.* **2015**, *11*, 655−666.
(36) Spezia, R.; Knecht, S.; Mennucci, B. Excited State Characterization of Carbonyl Containing Carotenoids: A Comparison between Single and Multireference Descriptions. *Phys. Chem. Chem. Phys.* **2017**, *19*, 17156−17166.
(37) Sashima, T.; Koyama, Y.; Yamada, T.; Hashimoto, H. The $1B_u^+$, $1B_u^-$, and $2A_g^-$ Energies of Crystalline Lycopene, β-Carotene, and Mini-9-β-Carotene as Determined by Resonance-Raman Excitation Profiles: Dependence of the $1B_u^-$ State Energy on the Conjugation Length. *J. Phys. Chem. B* **2000**, *104*, 5011−5019.
(38) Cerullo, G.; Polli, D.; Lanzani, G.; De Silvestri, S.; Hashimoto, H.; Cogdell, R. J. Photosynthetic Light Harvesting by Carotenoids: Detection of an Intermediate Excited State. *Science* **2002**, *298*, 2395−2398.
(39) Polli, D.; Cerullo, G.; Lanzani, G.; De Silvestri, S.; Yanagi, K.; Hashimoto, H.; Cogdell, R. J. Conjugation Length Dependence of Internal Conversion in Carotenoids: Role of the Intermediate State. *Phys. Rev. Lett.* **2004**, *93*, 163002.
(40) Ostroumov, E.; Müller, M. G.; Marian, C. M.; Kleinschmidt, M.; Holzwarth, A. R. Electronic Coherence Provides a Direct Proof for Energy-Level Crossing in Photoexcited Lutein and β-Carotene. *Phys. Rev. Lett.* **2009**, *103*, 108302.
(41) Ostroumov, E. E.; Mulvaney, R. M.; Cogdell, R. J.; Scholes, G. D. Broadband 2D Electronic Spectroscopy Reveals a Carotenoid Dark State in Purple Bacteria. *Science* **2013**, *340*, 52−56.
(42) Tavan, P.; Schulten, K. Electronic Excitations in Finite and Infinite Polyenes. *Phys. Rev. B: Condens. Matter* **1987**, *36*, 4337−4358.
(43) Ghosh, S.; Bishop, M. M.; Roscioli, J. D.; Mueller, J. J.; Shepherd, N. C.; LaFountain, A. M.; Frank, H. A.; Beck, W. F. Femtosecond Heterodyne Transient-Grating Studies of Nonradiative Decay of the S_2 $(1^1B_u^+)$ State of β-Carotene: Contributions from Dark Intermediates and Double-Quantum Coherences. *J. Phys. Chem. B* **2015**, *119*, 14905−14924.
(44) Ghosh, S.; Bishop, M. M.; Roscioli, J. D.; LaFountain, A. M.; Frank, H. A.; Beck, W. F. Femtosecond Heterodyne Transient Grating Studies of Nonradiative Deactivation of the S_2 $(1^1B_u^+)$ State of Peridinin: Detection and Spectroscopic Assignment of an Intermediate in the Decay Pathway. *J. Phys. Chem. B* **2016**, *120*, 3601−3614.
(45) Ghosh, S.; Roscioli, J. D.; Bishop, M. M.; Gurchiek, J. K.; LaFountain, A. M.; Frank, H. A.; Beck, W. F. Torsional Dynamics and Intramolecular Charge Transfer in the S_2 $(1^1B_u^+)$ Excited State of Peridinin: A Mechanism for Enhanced Mid-Visible Light Harvesting. *J. Phys. Chem. Lett.* **2016**, *7*, 3621−3626.
(46) Sanchez-Galvez, A.; Hunt, P.; Robb, M. A.; Olivucci, M.; Vreven, T.; Schlegel, H. B. Ultrafast Radiationless Deactivation of Organic Dyes: Evidence for a Two-State Two-Mode Pathway in Polymethine Cyanines. *J. Am. Chem. Soc.* **2000**, *122*, 2911−2924.
(47) Ben-Nun, M.; Martínez, T. J. Photodynamics of Ethylene: Ab Initio Studies of Conical Intersections. *Chem. Phys.* **2000**, *259*, 237−248.
(48) de Weerd, F. L.; van Stokkum, I. H. M.; van Grondelle, R. Subpicosecond Dynamics in the Excited State Absorption of All-*trans*-β-Carotene. *Chem. Phys. Lett.* **2002**, *354*, 38−43.
(49) Bonačić-Koutecký, V.; Bruckmann, P.; Hiberty, P.; Koutecký, J.; Leforestier, C.; Salem, L. Sudden Polarization in the Zwitterionic Z1 Excited States of Organic Intermediates. Photochemical Implications. *Angew. Chem., Int. Ed.* **1975**, *14*, 575−576.
(50) Bonačić-Koutecký, V.; Koutecký, J.; Michl, J. Neutral and Charged Biradicals, Zwitterions, Funnels in S_1, and Proton Translocation: Their Role in Photochemistry, Photophysics, and Vision. *Angew. Chem., Int. Ed.* **1987**, *26*, 170−189.
(51) Michl, J.; Bonačić-Koutecký, V. *Electronic Aspects of Organic Photochemistry*; Wiley, 1990.
(52) Liebel, M.; Schnedermann, C.; Kukura, P. Vibrationally Coherent Crossing and Coupling of Electronic States during Internal Conversion in β-Carotene. *Phys. Rev. Lett.* **2014**, *112*, 198302.
(53) Birge, R. R.; Zgierski, M. Z.; Serrano-Andres, L.; Hudson, B. S. Transition Dipole Orientation of Linear Polyenes: Semiempirical Models and Extrapolation to the Infinite Chain Limit. *J. Phys. Chem. A* **1999**, *103*, 2251−2255.
(54) Dolan, P. M.; Miller, D.; Cogdell, R. J.; Birge, R. R.; Frank, H. A. Linear Dichroism and the Transition Dipole Moment Orientation of the Carotenoid in the LH2 Antenna Complex in Membranes of *Rhodopseudomonas Acidophila* Strain 10050. *J. Phys. Chem. B* **2001**, *105*, 12134−12142.
(55) Enriquez, M. M.; Fuciman, M.; LaFountain, A. M.; Wagner, N. L.; Birge, R. R.; Frank, H. A. The Intramolecular Charge Transfer State in Carbonyl-Containing Polyenes and Carotenoids. *J. Phys. Chem. B* **2010**, *114*, 12416−12426.
(56) Gurchiek, J. K.; Bao, H.; Domínguez-Martín, M. A.; McGovern, S. E.; Marquardt, C. E.; Roscioli, J. D.; Ghosh, S.; Kerfeld, C. A.; Beck, W. F. Fluorescence and Excited-State Conformational Dynamics of the Orange Carotenoid Protein. *J. Phys. Chem. B* **2018**, *122*, 1792−1800.
(57) Jeevarajan, A. S.; Kispert, L. D.; Avdievich, N. I.; Forbes, M. D. E. Role of Excited Singlet State in the Photooxidation of Carotenoids: A Time-Resolved Q-Band EPR Study. *J. Phys. Chem.* **1996**, *100*, 669−671.
(58) Mortensen, A.; Skibsted, L. H. Kinetics of Photobleaching of β-Carotene in Chloroform and Formation of Transient Carotenoid Species Absorbing in the Near Infrared. *Free Radical Res.* **1996**, *25*, 355−368.
(59) Zhang, J.-P.; Fujii, R.; Koyama, Y.; Rondonuwu, F. S.; Watanabe, Y.; Mortensen, A.; Skibsted, L. H. The $1B_u$-Type Singlet State of β-Carotene as a Precursor of the Radical Cation Found in Chloroform Solution by Sub-Picosecond Time-Resolved Absorption Spectroscopy. *Chem. Phys. Lett.* **2001**, *348*, 235−241.
(60) Becke, A. D. Density-functional Thermochemistry. III. The Role of Exact Exchange. *J. Chem. Phys.* **1993**, *98*, 5648−5652.
(61) Stephens, P. J.; Devlin, F. J.; Chabalowski, C. F.; Frisch, M. J. Ab Initio Calculation of Vibrational Absorption and Circular Dichroism Spectra Using Density Functional Force Fields. *J. Phys. Chem.* **1994**, *98*, 11623−11627.
(62) Frisch, M. J.; Trucks, G. W.; Schlegel, H. B.; Scuseria, G. E.; Robb, M. A.; Cheeseman, J. R.; Scalmani, G.; Barone, V.; Petersson, G. A.; Nakatsuji, H. et al. *Gaussian 16* Rev. A.01; Wallingford, CT, 2016.

https://dx.doi.org/10.1021/acs.jpcb.0c06961
J. Phys. Chem. B 2020, 124, 9029−9046

(63) Yanai, T.; Tew, D. P.; Handy, N. C. A New Hybrid Exchange–correlation Functional Using the Coulomb-Attenuating Method (CAM-B3LYP). *Chem. Phys. Lett.* **2004**, *393*, 51–57.
(64) Lu, T.; Chen, F. Multiwfn: A Multifunctional Wavefunction Analyzer. *J. Comput. Chem.* **2012**, *33*, 580–592.
(65) Fleming, G. R.; Cho, M. Chromophore-Solvent Dynamics. *Annu. Rev. Phys. Chem.* **1996**, *47*, 109–134.
(66) Saito, S.; Tasumi, M.; Eugster, C. H. Resonance Raman Spectra (5800–40 cm^{-1}) of All-*trans* and 15-*cis* Isomers of *β*-Carotene in the Solid State and in Solution. Measurements with Various Laser Lines from Ultraviolet to Red. *J. Raman Spectrosc.* **1983**, *14*, 299–309.
(67) Sverdlov, L. M.; Kovner, M. A.; *Krai. Vibrational Spectra of Polyatomic Molecules*; John Wiley & Sons, 1973.
(68) Cantor, C. R.; Schimmel, P. R. *Biophysical Chemistry. Part II: Techniques for the Study of Biological Structure and Function*; W. H. Freeman and Company: San Francisco, 1980.
(69) Lakowicz, J. R. *Principles of Fluorescence Spectroscopy*, 3rd ed.; Springer: New York, 2006.
(70) Yu, A.; Tolbert, C. A.; Farrow, D. A.; Jonas, D. M. Solvatochromism and Solvation Dynamics of Structurally Related Cyanine Dyes. *J. Phys. Chem. A* **2002**, *106*, 9407–9419.
(71) Ejder, E. Methods of Representing Emission, Excitation, and Photoconductivity Spectra. *JOSA* **1969**, *59*, 223–224.
(72) Melhuish, W. H. Absolute Spectrofluorimetry. *J. Res. Natl. Bur. Stand.* **1972**, *76A*, 547–560.
(73) Mooney, J.; Kambhampati, P. Get the Basics Right: Jacobian Conversion of Wavelength and Energy Scales for Quantitative Analysis of Emission Spectra. *J. Phys. Chem. Lett.* **2013**, *4*, 3316–3318.
(74) Andersson, P. O.; Bachilo, S. M.; Chen, R.-L.; Gillbro, T. Solvent and Temperature Effects on Dual Fluorescence in a Series of Carotenes. Energy Gap Dependence of the Internal Conversion Rate. *J. Phys. Chem.* **1995**, *99*, 16199–16209.
(75) Ricci, M.; Torre, R.; Foggi, P.; Kamalov, V.; Righini, R. Molecular Dynamics of *β*-Carotene in Solution by Resonance Enhanced Optical Kerr Effect. *J. Chem. Phys.* **1995**, *102*, 9537.
(76) Bondarev, S. L.; Bachilo, S. M.; Dvornikov, S. S.; Tikhomirov, S. A. $S_2 \rightarrow S_0$ Fluorescence and Transient $S_n \leftarrow S_1$ Absorption of All-*trans*-*β*-Carotene in Solid and Liquid Solutions. *J. Photochem. Photobiol., A* **1989**, *46*, 315–322.
(77) Shreve, A. P.; Trautman, J. K.; Owens, T. G.; Albrecht, A. C. Determination of the S_2 Lifetime of *β*-Carotene. *Chem. Phys. Lett.* **1991**, *178*, 89–96.
(78) Siano, D. B.; Metzler, D. E. Band Shapes of the Electronic Spectra of Complex Molecules. *J. Chem. Phys.* **1969**, *51*, 1856–1861.
(79) Dickson, A. D.; Mills, I. M.; Crawford, B. Vibrational Intensities. VIII. CH_3 and CD_3 Chloride, Bromide, and Iodide. *J. Chem. Phys.* **1957**, *27*, 445–455.
(80) Durig, J. R.; Kizer, K. L.; Karriker, J. M. Spectra and Structure of Small Ring Compounds. XXXVI. 2-Methyl-1,3-Dioxolane; 2-Methyl-1,3-Dioxolane-d_4; 2-Methyltetrahydrofuran; and Methylcyclopentane. *J. Raman Spectrosc.* **1973**, *1*, 17–45.
(81) Shimanouchi, T.. *Tables of Molecular Vibrational Frequencies Consolidated Volume I*; National Bureau of Standards, 1972; pp. 1–160.
(82) Kochendoerfer, G. G.; Mathies, R. A. Spontaneous Emission Study of the Femtosecond Isomerization Dynamics of Rhodopsin. *J. Phys. Chem.* **1996**, *100*, 14526–14532.
(83) Norden, B.; Lindblom, G.; Jonas, I. Linear Dichroism Spectroscopy as a Tool for Studying Molecular Orientation in Model Membrane Systems. *J. Phys. Chem.* **1977**, *81*, 2086–2093.
(84) Niedzwiedzki, D. M.; Enriquez, M. M.; Lafountain, A. M.; Frank, H. A. Ultrafast Time-Resolved Absorption Spectroscopy of Geometric Isomers of Xanthophylls. *Chem. Phys.* **2010**, *373*, 80–89.
(85) Andersson, P. O.; Gillbro, T.; Ferguson, L.; Cogdell, R. J. Absorption Spectral Shifts of Carotenoids Related to Medium Polarizability. *Photochem. Photobiol.* **1991**, *54*, 353–360.
(86) Qu, G.; Xin, M.; Jia, Q.; Cai, P.; Jin, G.; Zhou, Y.; Liu, C.; Tan, Y.; Zhang, Y.; Yao, Z.; et al. Resonance Raman Features All-*trans*-*β*-Carotene during Phase Transition and Theoretical Investigation Analysis. *Optik* **2019**, *185*, 191–198.
(87) Ling, A. C.; Willard, J. E. Viscosities of Some Organic Glasses Used as Trapping Matrixes. *J. Phys. Chem.* **1968**, *72*, 1918–1923.
(88) Warshel, A. Bicycle-Pedal Model for the First Step in the Vision Process. *Nature* **1976**, *260*, 679–683.
(89) Liu, R. S.; Asato, A. E. The Primary Process of Vision and the Structure of Bathorhodopsin: A Mechanism for Photoisomerization of Polyenes. *Proc. Natl. Acad. Sci. U. S. A.* **1985**, *82*, 259–263.
(90) Liu, R. S. H. Photoisomerization by Hula-Twist: A Fundamental Supramolecular Photochemical Reaction. *Acc. Chem. Res.* **2001**, *34*, 555–562.
(91) Ostroumov, E. E.; Müller, M. G.; Reus, M.; Holzwarth, A. R. On the Nature of the "Dark S*" Excited State of *β*-Carotene. *J. Phys. Chem. A* **2011**, *115*, 3698–3712.
(92) Andersson, P. O.; Gillbro, T.; Asato, A. E.; Liu, R. S. H. Temperature and Viscosity Sensitive S_1 Emission from a Highly Substituted Triene. *Chem. Phys. Lett.* **1995**, *235*, 76–82.
(93) Menter, J. M. Temperature Dependence of Collagen Fluorescence. *Photochem. Photobiol. Sci.* **2006**, *5*, 403–410.
(94) Brocklehurst, B.; Young, R. N. Fluorescence Anisotropy Decays and Viscous Behaviour of 2-Methyltetrahydrofuran. *J. Chem. Soc., Faraday Trans.* **1994**, *90*, 271.
(95) Palings, I.; Van den Berg, E. M. M.; Lugtenburg, J.; Mathies, R. A. Complete Assignment of the Hydrogen Out-of-Plane Wagging Vibrations of Bathorhodopsin: Chromophore Structure and Energy Storage in the Primary Photoproduct of Vision. *Biochemistry* **1989**, *28*, 1498–1507.
(96) Schapiro, I.; Ryazantsev, M. N.; Frutos, L. M.; Ferré, N.; Lindh, R.; Olivucci, M. The Ultrafast Photoisomerizations of Rhodopsin and Bathorhodopsin Are Modulated by Bond Length Alternation and HOOP Driven Electronic Effects. *J. Am. Chem. Soc.* **2011**, *133*, 3354–3364.
(97) Andersson, P. O.; Gillbro, T.; Asato, A. E.; Liu, R. S. H. Dual Singlet State Emission in a Series of Mini-Carotenes. *J. Lumin.* **1992**, *51*, 11–20.
(98) Malhado, J. P.; Spezia, R.; Hynes, J. T. Dynamical Friction Effects on the Photoisomerization of a Model Protonated Schiff Base in Solution. *J. Phys. Chem. A* **2011**, *115*, 3720–3735.
(99) Minezawa, N.; Gordon, M. S. Optimizing Conical Intersections by Spin-Flip Density Functional Theory: Application to Ethylene. *J. Phys. Chem. A* **2009**, *113*, 12749–12753.
(100) Kochendoerfer, G. G.; Mathies, R. A. Ultrafast Spectroscopy of Rhodopsins—Photochemistry at Its Best! *Isr. J. Chem.* **1995**, *35*, 211–226.
(101) Birge, R. R. Nature of the Primary Photochemical Events in Rhodopsin and Bacteriorhodopsin. *Biochim. Biophys. Acta* **1990**, *1016*, 293–327.
(102) Kukura, P.; McCamant, D. W.; Yoon, S.; Wandschneider, D. B.; Mathies, R. A. Structural Observation of the Primary Isomerization in Vision with Femtosecond-Stimulated Raman. *Science* **2005**, *310*, 1006–1009.
(103) Schnedermann, C.; Liebel, M.; Kukura, P. Mode-Specificity of Vibrationally Coherent Internal Conversion in Rhodopsin during the Primary Visual Event. *J. Am. Chem. Soc.* **2015**, *137*, 2886–2891.
(104) Hasson, K. C.; Gai, F.; Anfinrud, P. A. The Photoisomerization of Retinal in Bacteriorhodospin: Experimental Evidence for a Three-State Model. *Proc. Natl. Acad. Sci. U. S. A.* **1996**, *93*, 15124–15129.
(105) Song, L.; El-Sayed, M. A. Primary Step in Bacteriorhodopsin Photosynthesis: Bond Stretch Rather than Angle Twist of Its Retinal Excited-State Structure. *J. Am. Chem. Soc.* **1998**, *120*, 8889–8890.
(106) Lewis, A.; Spoonhower, J. P.; Perreault, G. J. Observation of Light Emission from a Rhodopsin. *Nature* **1976**, *260*, 675.
(107) Kouyama, T.; Kinosita, K. J.; Ikegami, A. Excited-State Dynamics of Bacteriorhodopsin. *Biophys. J.* **1985**, *47*, 43–54.
(108) Haran, G.; Wynne, K.; Xie, A.; He, Q.; Chance, M.; Hochstrasser, R. M. Excited State Dynamics of Bacteriorhodopsin

https://dx.doi.org/10.1021/acs.jpcb.0c06961
J. Phys. Chem. B 2020, 124, 9029–9046

Revealed by Transient Stimulated Emission Spectra. *Chem. Phys. Lett.* **1996**, *261*, 389−395.
(109) Nosrati, M.; Berbasova, T.; Vasileiou, C.; Borhan, B.; Geiger, J. H. A Photoisomerizing Rhodopsin Mimic Observed at Atomic Resolution. *J. Am. Chem. Soc.* **2016**, *138*, 8802−8808.
(110) Ghanbarpour, A.; Nairat, M.; Nosrati, M.; Santos, E. M.; Vasileiou, C.; Dantus, M.; Borhan, B.; Geiger, J. H. Mimicking Microbial Rhodopsin Isomerization in a Single Crystal. *J. Am. Chem. Soc.* **2019**, *141*, 1735−1741.
(111) Bautista, J. A.; Connors, R. E.; Raju, B. B.; Hiller, R. G.; Sharples, F. P.; Gosztola, D.; Wasielewski, M. R.; Frank, H. A. Excited State Properties of Peridinin: Observation of a Solvent Dependence of the Lowest Excited Singlet State Lifetime and Spectral Behavior Unique among Carotenoids. *J. Phys. Chem. B* **1999**, *103*, 8751−8758.
(112) Kirilovsky, D. Photoprotection in Cyanobacteria: The Orange Carotenoid Protein (OCP)-Related Non-Photochemical-Quenching Mechanism. *Photosynth. Res.* **2007**, *93*, 7−16.
(113) Ghosh, S.; Bishop, M. M.; Roscioli, J. D.; LaFountain, A. M.; Frank, H. A.; Beck, W. F. Excitation Energy Transfer by Coherent and Incoherent Mechanisms in the Peridinin−Chlorophyll *a* Protein. *J. Phys. Chem. Lett.* **2017**, *8*, 463−469.

NOTE ADDED AFTER ASAP PUBLICATION

This paper was published ASAP on October 2, 2020, and was reposted on October 15, 2020 with revised Supporting Information.

https://dx.doi.org/10.1021/acs.jpcb.0c06961
J. Phys. Chem. B 2020, 124, 9029−9046